Impact of RPS15 mutations on the development and progression of chronic lymphocytic leukemia

Impact of *RPS15* mutations on the development and progression of chronic lymphocytic leukemia

Peyton Waddicor

A Thesis Submitted to the Faculty

of The Harvard Medical School

in Partial Fulfillment of the Requirements

for the Degree of Master of Medical Sciences in Immunology

Harvard University

Boston, Massachusetts.

May 2021

Thesis advisor: Dr. Catherine Wu Peyton Waddicor

Abstract

Large-scale sequencing of chronic lymphocytic leukemia (CLL) has uncovered vast genetic heterogeneity and novel putative CLL driver mutations, including in the ribosomal protein S15 (*RPS15)*. RPS15, a component of the 40S subunit of the ribosome, is a part of the mRNA decoding site in actively translating ribosomes and has been directly implicated in the regulation of p53 stability via the MDMX/MDM2 axis. We generated a human CLL cell line harboring hotspot *RPS15* mutations and a conditional knock-in mouse model of the most frequent *RPS15*-S138F mutation. We further modeled the common co-occurrence of *RPS15* mutation and *TP53* deletion identified in patient samples by developing 'double-mutant' cell lines and mice. Through this work, we demonstrated that *RPS15* mutations alter B cell development, signaling and immune function. Comparative analysis at the transcriptional, translational and proteomic level revealed a strong upregulation of the MYC pathway in *RPS15* mutant cells, possibly mediated by upregulation of Zap70. MYC activity increased further in the setting of *TP53* deletion, suggesting that loss of *TP53* enables *RPS15* mutant-mediated MYC activation and disease development. Finally, we demonstrate that *RPS15* and *TP53* mutation alone can drive CLL-like disease, and that *RPS15* and *TP53* double mutants develop disease that is morphologically and functionally distinct from either mutation alone.

Table of Contents

LIST OF FIGURES

LIST OF TABLES

Acknowledgments

I would like to begin by thanking my PI, Catherine Wu, for her exceptional mentorship, support and continuous demonstration of how much she values science, but even further how much she cares about the members of her lab. I would like to thank my many mentors within the lab, Anat Biran and Elisa Ten Hacken for their guidance over the past year. And chiefly, Catherine Gutierrez for her dedication to science, mentorship and this project. I would not have been able to complete this thesis without her support. I would like to thank all members of the Wu lab for their friendship and support during this crazy year. I would especially like to express appreciation for Beth Witten, Leah Billington, Lucas Pomerance and Nathan Dangle for constant technical support. Doris Fu and Tamara Ouspenskaia for exceptional computational contributions and knowledge. As well as Donna Neuberg for invaluable feedback and statistical expertise. I would like to thank Dana Farber Cancer Institute for their dedication to safety and valuing their employees throughout the pandemic.

Thank you to the devoted faculty and staff within the HMS Master's Immunology program, Shiv Pillai, Michael Carroll, Gavin Porter and Selina Sarmiento. All of whom have shown dedication and encouragement to the students of our class. I would also like to thank my classmates who have stuck together to overcome unprecedented obstacles throughout our master's degree. In particular, Kimmy Ye and Shivan Lala who have provided untold amounts of friendship and mental support since we met in 2018.

Lastly, I would like to acknowledge my parents, Bonnie and Bob Waddicor, who have made me feel that my dreams and pursuits were limitless and encouraged me to follow my heart.

And an immense thank you to my partner and biggest supporter, James Conley, without whom I would not have made it through this program.

Chapter 1: Background

1.1 Introduction

While advancements in the understanding of oncology have improved the survival outcomes across a number of cancers, our comprehension of malignant cells is still far from what is necessary to relieve the population of the devastation is associated with a cancer diagnosis. One overarching question that remains is by what means do mutations drive oncogenesis. In addition, what is the impact of mutations in combination on the progression of disease. Further work is necessary to pair altered genes in cancer with the phenotype of disease.

Chronic Lymphocytic Leukemia (CLL), a mature B cell malignancy, has been at the forefront of genetic discovery and understanding clonal diversity within a tumor population. This is largely due to the accessibility of high-purity leukemic cells from peripheral blood and relative indolence, which allows for longitudinal sampling throughout the course of disease. Additionally, variability within disease course across patients enables monitoring of molecular characteristics that associate with prognosis and clinical outcomes[3]. Recent advances in sequencing technologies have allowed staging classifications and clinical prognostic tests to be complemented by CLL genetics and functional biology, providing improved patient prognostics and treatment plans[1].

In 2015, large-scale whole-exome and -genome sequencing (WES/WGS) of CLL has uncovered more than 50 recurrently mutated genes and identified putative drivers of CLL[1,4] In each of these studies, the groups analyzed genomic data from cohorts of over 500 patients with CLL. From this information, large databases detailing patient demographics, treatment information and cancer genomes have been compiled from multiple hospitals around the world. The accumulation of multiple patient cohorts has since allowed for increased sensitivity in the identification of mutational drivers[5,6].

The analysis of larger patient groups helps to reveal a number of putative drivers that occur more infrequently, yet may play a critical role in disease progression. While many of the mutations were identified in less than 10% of patients, they affect genes in key cellular pathways that become dysregulated in leukemic cells[1]. A number of genes identified in the 2015 study have been identified as novel putative drivers of CLL, these include mutations in the *IKZF3, MGA* and *RPS15* genes. While our understanding of the genetic components of CLL has grown, much remains unknown as to the functional and mechanistic role that these drivers have in influencing disease, and how they may work in conjunction with co-mutations in disease development and progression.

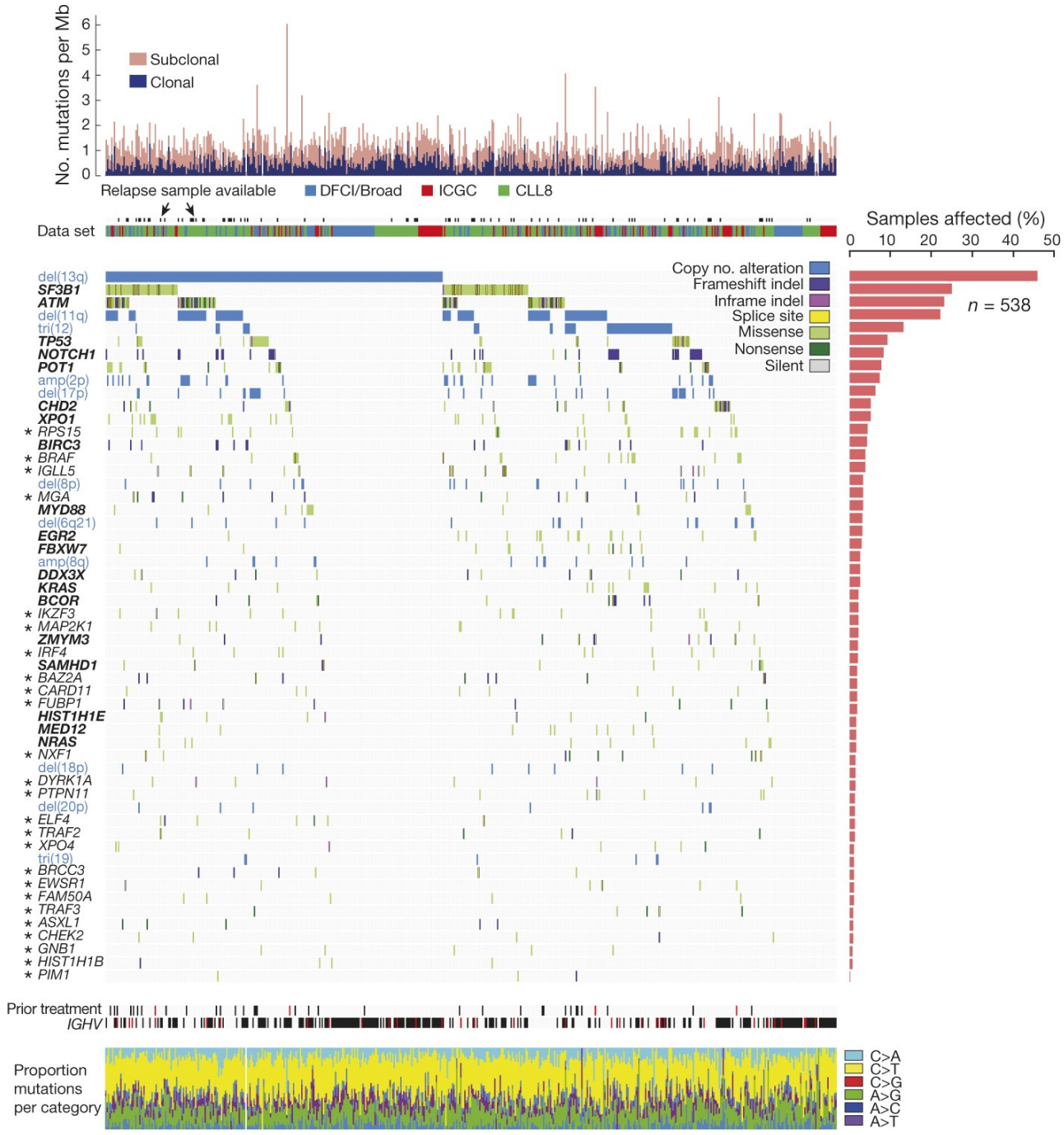

Supplementary Figure 1 Identification of novel putative drivers in CLL[1]

Somatic mutation and copy number alteration information for 55 putative driver genes identified from 538 primary patient samples derived from 3 cohorts that were analyzed by WES. Blue labels, recurrent somatic CNAs; bold labels, putative CLL cancer genes previously identified in Landau et. al 2013, asterisked labels, additional cancer-associated genes identified in this study. Samples were annotated for *IGHV* status (black, mutated; white unmutated; red, unknown), and for exposure to

therapy before sampling (black, previous therapy; white, no previous therapy; red, unknown previous treatment status).[1]

1.2 Chronic lymphocytic leukemia

Chronic lymphocytic leukemia (CLL) is a mature B cell leukemia characterized by the expansion of small B lymphocytes that express CD5+ and CD23+ surface markers[7]. The most prevalent adult leukemia in the United States and Europe, CLL has an incidence of 4.7 new cases per 100,000 individuals[8] and a median age of diagnosis of 70[9], with a male predominance of 1.3 to 1[10].

While there have been ongoing advancements to screening and treatment, CLL remains an incurable disease. Overall survival (OS) is dependent on stage of disease as well a number of biologic factors of the malignant cells, such as immunoglobulin heavy chain V rearrangement (IGHV) status. The largest contributors of death in patients is secondary infection as a result of humoral depression and immune suppression as a result of treatment, accounting for 50-60% of CLL deaths[11].

A major prognostic factor for CLL relies on whether the IGHV region of the B cell receptor (BCR) has undergone somatic hypermutation (SHM), characterized as IGHV mutated or unmutated, the latter indicating a worse disease prognosis[12]. Additionally, stages of CLL have been broken down into subcategories of risk, Rai Stages 0-IV. This system divides patients who only display lymphocytosis as having low-risk CLL (Rai Stage 0-I), those with palpable lymph nodes or hepatosplenomegaly as having intermediate-risk disease (Rai Stages II-III), and those presenting with anemia or thrombocytopenia as high-risk disease (Rai Stage IV)[13]. Given its highly variable presentation and disease course, patients with CLL are often tested for a number of other prognostic factors. These have historically included lymphocyte doubling time (LDT) as an

indication of disease severity, with a LDT of less than 12 months considered less favorable than a LDT of greater than 12 months[14]. Other laboratory prognostic tests for CLL include measuring levels of beta-2-Microglobulin (β2M) and soluble CD antigens in the blood, with increased levels being associated with active CLL disease and shorter OS, the time between diagnosis and death, and disease free progression (DFP)[14]. DFP or progression free survival (PFS) is the time between treatment and the worsening of disease, commonly used in clinical trials to report the efficacy of treatments[15]. Increased expression of tyrosine kinase ZAP70, as measured by flow cytometry, has been also associated with an unfavorable disease course[16]. Finally, presence of CLL cells in the bone marrow (BM), as determined by BM biopsy, can be used to predict severity and disease progression[14]. This marks disease progression because CLL cells are most commonly found in the circulation and are thought to originate from a mature B cell that has left the BM compartment. BM infiltration indicates increased CLL burden and entry into other immune cell compartments[17].

Until 2013, standard treatment for CLL consisted of chemoimmunotherapy, namely the combination of three therapeutic agents, fludarabine (a fluorinated purine nucleoside analogue which inhibits DNA synthesis by interfering with ribonucleotide reductase and DNA polymerase), cyclophosphamide (drives apoptosis through crosslinking of DNA) and rituximab (an anti-CD20 monoclonal antibody), known as (FCR).

In the past decade, randomized clinical trials have tested different treatment combinations and found improved survival with novel targeted agents, including ibrutinib, idelalisib and venetoclax[12,18]. One common targeted therapeutic acts by targeting B cell receptor (BCR) signaling, a core signaling pathway in CLL. BCR signaling plays a critical role in the proliferations of CLL cells, it can induced by antigen or ligand-independent ("tonic" BCR signaling), which generates a signaling cascade that normally cause B cell proliferation, differentiation, and

antibody production[19]. One such drug is ibrutinib, the first-in-class inhibitor of Bruton Tyrosine Kinaase (BTK), a downstream mediator of the BCR signaling cascade, also in this class is acalabrutinib, a second generation agent with higher selectivity for BTK[20]. These act by inducing cell lysis of a fraction of CLL cells, and mobilize CLL cells from lymphoid tissue and into peripheral blood[21]. Other BCR signaling inhibitors include idelalisib and copanlisib that target phosphatidylinositol 3-kinase (PI3K)[22]. A number of randomized clinical trials have demonstrated improved efficacy of these inhibitors in combination with the chemotherapy agent chlorambucil, with combination treatment exhibiting longer progression free survival[18,20].

Other agents target cell death by means of inducing apoptosis. The apoptotic protein, BCL2 is located in the outer mitochondrial membrane that inhibits cell death by acting as an inhibitor against pro-apoptotic proteins. A common, FDA approved, targeted therapy used to treat CLL is the BCL2 inhibitor, Venetoclax. CLL patients often exhibit increases in BCL2 expression[23]. Venetoclax acts as an alternative to BTK or other kinase inhibitors, however clinical trials have shown a high efficacy of treatment when used in combination or sequentially[22].

Other treatment options include cellular therapies. There has been some clinical progress with autologous chimeric antigen receptor (CAR) T cell therapy targeted against CD19. However, these trials have shown low response rates[24]. A number of trials are looking at efficacy of combinations treatments with cell therapy[25]. Currently allogeneic hematopoietic stem cell transplant remains the most common cell therapy for CLL, with around half of treated patients exhibiting long term remission and survival[26].

Even with a number of available treatments, many patients experience persistence of disease. In 2-10% of patients, CLL undergoes Richter's transformation, a syndrome defined by the rapid transformation of CLL into an aggressive, large cell lymphoma. While research into the

drivers and treatment of Richter's syndrome is an active field, it is a terminal diagnosis with the length of survival ranging from 8-14 months[27].

The advent of next generation sequencing has mediated analysis of the genetic makeup of cancer cells. In CLL, it has elucidated recurring mutations that may play a role in disease progression and therapeutic resistance, leading to aggressive relapse. Further studies to understand the underlying mechanisms that resist targeted therapies could aid in finally curing CLL as a whole. While our understanding of the genetic makeup of CLL has grown immensely, one limitation in the exploration of the phenotypic components has been modeling CLL in the lab.

1.3 Functional studies of putative driver mutations

In the dawn of genomic studies and the identifications of a large number of putative drivers in CLL, there is still a considerable amount that is unknown regarding the functional role of these mutations. While there are a limited number of human CLL cell line models (e.g. HG3, MEC1 and MEC2) they exbibit low fidelity to human disease. In addition, primary CLL samples have proven difficult to culture and therefore difficult for use in functional assays. While CLL is the expansion of a single cell type, it is influenced by the entire body, including organ microenvironment and immune factors, such as T cell interaction.

In order to gain the best understanding of mutational drivers, we have generated immunocompetent mouse models to further investigate the role of these recurrent aberrations in the development of CLL. The utilization of transgenic mouse models allows for the use of functional assays to understand the underlying mechanisms of dysregulation in the presence of genetic mutations. Through the use of these models, we can study systemic effects of disease progression. Additionally, CLL is a disease that predominantly affects the elderly population,

mouse models allow us to observe the impact of age on disease, while immortalized cell lines cannot[9,28].

Using readily available genetic manipulation techniques we are able to generate conditional knock-in of mutations into endogenous gene loci and models of heterozygous mutations within a physiologic context. One mouse model, generated in 2002 is the Eμ-TCL1 transgenic mouse, capable of driving aggressive CLL[29]. However, in the majority of CLL cases in patients behave as an indolent disease, making this an inadequate model for the study of CLL and how it develops[30]. Our group previously constructed a *in vivo* model with CLL-associated mutations *Atm* deletion and heterozygous *Sf3b1* mutation expressed in a restricted $CD19^{+}$ B cell context. This model yielded low penetrance CLL-like disease in mice and uncovered the role of *Sf3b1* mutations on BCR signaling that was further confirmed in human primary samples[28]. Following these findings, the lab has pursued generating additional *in vivo* models of recurrently mutated genes identified in CLL. These include mut-IKZF3 under the control of CD19+ expression and CRISPR targeted loss-of-function CLL lesions into B lineage cells of Cas9 transgenic mice[2,31].

This model, using hotspot mutation (L162R) in the IKAROS family zinc finger 3 (*IKZF3*) has been identified as a putative driver of CLL[32]. To study this putative driver further, our lab generated conditional knock-in mouse model with B cell-restricted expression of the *Ikzf3-L161R* mutation using the *Cd19*-Cre/loxP system that showed *IKZF3* mutations were capable of driving CLL in elderly mice that is consistent with features seen in human disease[2]. They found that altered DNA binding to BCR signaling-related target genes facilitated transactivation and enhanced BCR responsiveness. This highlighted the role of *IKZF3* mutations in BCR mediated oncogenesis and support the role of these mutations in the development of CLL[2]. These studies further emphasize

the promise of using B cell restricted mouse models in the characterization of driver mutations in CLL.

1.4 RPS15

In 2015, WGS sequencing patient cohorts identified Ribosomal Protein S15 (*RPS15)* as a novel putative driver of CLL. These mutations were identified in 5.3% of CLL patients and increased to 19.5% in relapsed CLL patients. Additionally, the presence of *RPS15* mutations is associated with poor disease prognosis and shorter progression free survival[33].

RPS15 is located on chromosome 19 and encodes a ribosomal protein that makes up a component of the 40S subunit of the ribosome[34]. Most *RPS15* mutations in CLL localize to an evolutionarily conserved region in the C-terminal tail recently shown to engage the mRNA decoding site of the ribosome and influence translational efficiency in yeast and human epithelial cell lines[1,33,35,36]. Most commonly, the mutations are missense mutations, isolated to a 14 amino acid region or the C-terminus, of the 145 amino acid protein (detailed in **Table 1**)[1,5]. Some of the most commonly identified mutations occur at residues that are commonly phosphorylated, changing to sites that can no longer accept a phospho- group (*ex: S138F, S139F and T136A,* **Table 1**). Nearly all *RPS15* mutations identified in patients were identified in patients with unmutated IGHV CLL (**Table 1**). *RPS15* has also been implicated in regulation of the MDM2-p53-MDMX pathway with effects on p53 stabilization[5,36]. As with many ribosomal protein mutations identified in cancer, *RPS15* mutations are frequently clonal, indicating a likely role as a foundational event in tumorigenesis[1].

These findings suggest that these mutations may be advantageous for the survival and progression of the leukemic cells. A number of studies have implicated the association of *RPS15* mutations with therapeutic resistance. In patients with CLL, *RPS15* mutations are enriched in the

setting of resistance and relapse to fludarabine-based chemotherapy, and have been implicated in ibrutinib resistance[5,36]. It is suggested that the resistance is mediated by its role in p53 stability and modification of DNA damage pathways, leading to BCR-signaling-independent growth[37]. *RPS15* mutations have also been noted to co-occur with *TP53* or del(17p) mutations in 36% of patients with CLL, and this combination associates with lower OS than for patients harboring either mutation alone[38]. RNA and ribosomal processing has been described as a key pathway in CLL, however the means by which RPS15 and other mutations disrupt these mechanisms is not well understood[32].

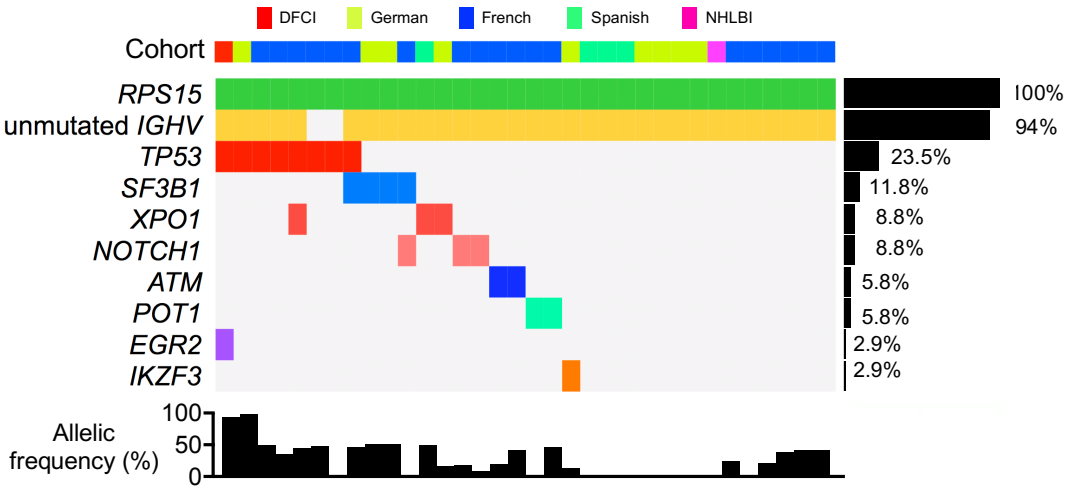

Supplementary Figure 2. Recurrent *RPS15* mutations identified in CLL WES and targeted sequencing studies. Genes and allelic frequency of co-mutations of patients with RPS15 mutations from 5 patient cohorts identified through WES or targeted sequencing. Left, shows percent of patients with identified co-mutation. Bottom, indicated the allelic frequency of RPS15 mutations within the patients' CLL population.

Table 1. *RPS15* mutations and co-mutations identified in CLL patient samples.

	Patient	*RPS15* mutation	Allelic Frequency (%)	IGHV status	Co-mutations (% Allelic Frequency)
Discovery Cohort	049TD	p.P131S	33.33333333	unmutated	
	139TD	p.S138F	23.4375	unmutated	
	270TD	p.G129V/ p.G129G	38.7, 38.7	unmutated	*XPO1* p.E571V (49.33%)
	812TD	del(STOP)	34.375	unmutated	
	CW-163	p.K145N	37	unmutated	*TP53* splice site (93.8%), *EGR2* p.E356K (45.5%)
	GCLL-0006	p.S138F	5.714285714	unmutated	*SF3B1* p.I704F (51.25%)
	GCLL-0045	p.T136A	10.95890411	unmutated	*IKZF3* p.L162R (13.8%)
	GCLL-0091	p.S138F	46.37681159	unmutated	
	GCLL-0143	p.K145*	52.77777778	unmutated	*SF3B1* p.K700E (50.9%)
	GCLL-0147	p.H137Y	15.30612245	unmutated	*SF3B1* p.D894G (12.6%), p.R775Q (16.8%), *XPO1* p.E571K (15.4%)
	GCLL-0150	p.G134R	18.18181818	unmutated	
	GCLL-0157	p.S138F	6.666666667	unmutated	
	GCLL-0234	p.G134R	31.4	unmutated	
	GCLL-0303	p.P131S	10.52631579	unmutated	*TP53* p.H179R (98.2%)
	NHLBI-0046	p.S139F	11.9	unmutated	
Validation Cohort	AVI_0001	p.S139F	50	unmutated	*TP53* p.T155I (91%)
	AVI_0002	p.S139F	36	unmutated	*TP53* p.Ser241Phe (32%), p.Val143fs (19.5%)
	AVI_0003	p.G134A	25	unmutated	
	AVI_0004	p.P131S	0.49	unmutated	
	AVI_0005	p.G132S	21	unmutated	
	AVI_0006	p.T136A	38	unmutated	
	AVI_0007	p.T136A	42	unmutated	
	AVI_0008	p.H137D	2	unmutated	*SF3B1* p.I704S (23%), *NOTCH* p.G2403fs (31%),
	AVI_0009	p.S138F	45	unmutated	*TP53* p.Cys275fs (8%), p.His214fs (4.2%), p.Lys139Glu (17.2%), p.Lys101Ter (2%); *XPO1* p.E571Q (36%)
	AVI_0010	p.P131S	42	unmutated	
	AVI_0011	p.H137Y	20	unmutated	*ATM* p.K468fs (9%)
	AVI_0012	p.S139F	42	unmutated	*ATM* c.6976-1G>T (95%)
	AVI_0013	p.T136A	48	unmutated	*POT1* p.Val46Asp (39%)
	AVI_0014	p.H137Y	47	unmutated	*POT1* p.Y242C (11%)
	AVI_0015	p.K145*	18	unmutated	*NOTCH1* p.P2514fs (26%)
	AVI_0016	p.S138F	9	unmutated	*NOTCH1* p.G2405* (47%), *POT1* p.G94R (42%)
	AVI_0017	p.T136A	ND	mutated	*TP53* p.A159P (3%)
	AVI_0018	p.T136A	ND	ND	*TP53* p.I251N (3.5%), p.P98R (2%)
	AVI_0019	p.P131S	47	unmutated	*TP53* p.P278H (63.6%), p.C277F (3.5%); *SF3B1* p.Gly742Asp (42%)

*ND = not determined

1.5 Ribosomal Protein Mutations

Translation is a tightly regulated mechanism within the cell. As such, cancers have been implicated in deregulating these systems in order to promote oncogenic activity[39].

One mechanism by which cancers harness translation is through mutations in ribosomal proteins (RPs). Protein synthesis is a highly energy consuming process, taking up ~20% of a cellular energy. Continuous proliferation within cancer cells requires high levels of protein synthesis, making this a key pathway for malignant cells[39]. Several RPs have been identified as recurrently mutated in a number of malignancies. utations have been found in RPL10, RPL5 and RPL11 in T-cell acute lymphoblastic leukemia, RPL22 in endometrial cancer, RPS20 in colorectal cancer and RPL5 in glioma[40]. Additionally, patients with Diamond-Blackfan anemia, a disease

caused by RP mutations have been described to be at high risk for the development of leukemias and solid tumors[33]. Ribosome biogenesis is a highly regulated process, RPs are generated in the cytoplasm and then move to the nucleus for the generation of ribosomes[41]. This is a tightly controlled process, if made in excess RPs are rapidly degraded and the loss of an RP may lead to an overall decrease in cellular ribosomes[40].

The exact mechanisms behind how RP mutations drive oncogenesis remain unknown. One prevailing theory involved cell cycle regulation by p53, a number of models have shown that alterations in RPs can lead to cell cycle arrest and apoptosis mediated by p53. One example of this was demonstrated in a mouse model with a knock down of *Rps6,* in which the embryonic lethality was observed due to p53-dependent cell cycle arrest and apoptosis[42]. A role for p53 mediated apoptosis has also been implicated in models containing *Rps19, Rps20,* and *Rpl22* mutations[43,44]. While these mutations demonstrate an inclination towards cell death, prevailing theories implicate that additional mutations that overcome p53 mediated arrest then progress towards a proliferative state[40]. Other proposed mechanisms indicate a role for alterations in translation. A model of *Rpl10* mutations in yeast cells, demonstrated degradation of the 60S ribosome and increases in ribosomal production to compensate. These alterations lead to defective ribosomes and detrimental changes to mRNA translation[45]. Changes to global translation have also been seen in functional studies of *RPS15* mutations. One group found that *RPS15* mutations in HEK293T and MEC-1 cells caused changes in translational fidelity and global changes within the proteome[36].

Chapter 2: Results

2.1 Introduction

Following the results of large-scale sequencing of CLL, which revealed several novel putative CLL driver mutations, we have investigated the functional characteristics of the putative driver mutations in the ribosomal protein *RPS15*. These mutations have been identified in 5.3% of CLL patients, and increasing to 19.5% in patients relapsing from frontline therapeutics[1,5]. These mutations often co-occur with genes related to DNA damage and RNA processing. One common co-mutation is heterozygous *TP53* alterations, seen in 36% of patients with *RPS15* mutation[5]. To study the functional aspects of *Rps15* mutations on translation and progression of CLL, we have a generated a *CD19*+ B cell restricted heterozygous and homozygous mut-*RPS15* mouse model. This conditional knock-in mouse model contains the most common mutation found in patients, *RPS15*-S138F mutation, in the presence and absence of *TP53* deletion. Additionally, we confirmed functional findings with patient samples and human CLL cell lines modeling four *RPS15* mutations (G134R, H137Y, S138F and S139F). Across cell lines *RPS15* mutant cells demonstrated reduced fitness that was partially rescued in the presence of TP53 mutations. We assessed the functional changes to B cells within the mouse models to understand the impact of these mutations. Longitudinal monitoring of *RPS15* and *TP53* mutant mouse cohorts for CLL-like signatures, showed that *RPS15* mutation alone can result in CLL-like disease, and that such disease may demonstrate changes in latency and morphology when in combination with *TP53* deletion. After observing their ability to drive CLL-like disease in mice, we assessed cancerous cells to further understand their phenotype and fidelity to CLL in patients. Comparative analysis at the transcriptional, translational and proteomic level revealed a strong upregulation of MYC activation

in *RPS15* mutant vs WT cells, with further activation in the setting of *TP53* deletion – an observation that was consistent across human and mouse models, and which collectively suggests that loss of a cell-cycle regulator, such as *TP53*, may enable *RPS15* mutant-mediated MYC activation and disease development.

These findings help to illuminate the mechanisms that may induce the accumulation of additional mutations leading to the development of CLL. These result further the understanding into how *Rps15* mutations cause cell dysregulation and may elucidate a candidate target for therapeutics. In addition, these may help uncover the mechanisms that are shared between ribosomal protein mutations and the generation of cell proliferative disease.

2.2 Materials and Methods

Cell culture

HG3 cells (DSMZ #ACC 765) were cultured in RPMI 1640 (Gibco #11875-093) with 15% fetal bovine serum (FBS) (Sigma-Aldrich), 1% GlutaMAX (Gibco, cat# 35050-061) and 1% penicillin-streptomycin (Life Technologies). Cells were incubated at 37 °C, 5% CO_2 and passaged every 48 hours. All subsets of the HG3 cell line were also cultured under these conditions. Cells were routinely tested for mycoplasma per the manufacturer's instructions (VenorGeM Mycoplasma Detection Kit; Sigma-Aldrich #MP0025).

Generation of mutant human CLL cell lines

Sleeping Beauty transposon plasmids carrying one of four RPS15 CLL mutations (G134R or c.400 G>C; H137Y or c.409C>T; S138F or c.413 C>T; and S139F or c.416 C>T) or the RPS15 WT gene were assembled by introducing gBlocks® (IDT) containing a Flag and HA tag upstream of the RPS15 WT or mutant coding sequence (codon optimized using the IDT Codon Optimization Tool), with SfiI overhangs on each end. Cloning was performed by digesting both the Sleeping Beauty inducible transposon plasmid pSBtet-GP (Addgene plasmid #60495) (CG37) (contains GFP and puromycin selection markers) and each gBlock with SfiI (#R0123S, New England Biolabs). To generate RPS15 mutant HG3 cell lines, HG3 cells were electroporated with 15 µg of pCMV(CAT)T7-SB100 (transposase, Addgene #34879) and 15 µg of each of the mutant transposon vectors. Successfully transposed cells were purified twice by FACS post-nucleofection.

To generate cells compatible with the CRISPR-Cas9 system, lentivirus was generated by co-transfection of LentiCas9-Blast (Addgene #52692)[46] along with pMD2.G (Addgene #12259) and psPAX2 (Addgene #12260) into HEK 293T using Lipofectamine 2000® (Life Technologies). Supernatant containing lentiviral particles was collected at 48 and 72 hours and concentrated using Lenti-X (Clontech). HG3 cells were transduced with fresh lentivirus in the presence of 8 μg/mL polybrene and selected by blasticidine (20 μg/ml) for two weeks and Cas9 activity was tested using a previously reported system[47,48].To generate *TP53* K/O cell lines, sgRNAs were designed using the online CRISPR design tool (http://crispr.mit.edu/) to target *TP53*. The selection of the sgRNAs was based on choosing those of highest efficiency to target the gene of interest and with the lowest predicted off-targets effects. The sgRNA targeting *TP53* (5'-CCATTGTTCAATATCGTCCG-3') was cloned into pLKO5.sgRNA.EFS.tRFP (Addgene_#57823)[49]. Cloning was carried out as previously described and lentivirus was generated as described above[50]. Cas9-expressing HG3 cells were transduced with the above *TP53*-targeting construct and RFP+ cells were flow-sorted as single cells into 96-well plates. To confirm CRISPR editing of the *TP53* loci, gDNA was extracted using the QIAampDNA Micro Kit (Qiagen) following the manufacturer's instructions. PCR was performed using primers flanking the target sites for the sgRNAs (Forward: AGACCTGTGGGAAGCGAAAA; Reverse: GACAGGAAGCCAAAGGGTGA). For screening the loss-of-function mutations, PCR products were purified using High Pure PCR Product Purification Kit (Roche) and resulting indels at the expected locations were confirmed by Sanger sequencing. The efficiency of the sgRNAs was assessed by Tracking of Indels by Decomposition (TIDE) software (https://tide-calculator.nki.nl; Netherlands Cancer Institute)[51]. Western blots were performed to confirm loss of p53 expression as described below (**Western Blot**).

Pyrosequencing

Relative transcript expression of the *RPS15* mutant allele compared to the wild-type was quantified by cDNA pyrosequencing as previously described[28]. Biotinylated amplicons were generated via cDNA synthesis and PCR amplification of transcripts surrounding the site of *RPS15*-S138F human and mouse mutation. Immobilized biotinylated single-stranded DNA fragments were isolated per the manufacturer's protocol (Pyromark Gold Q96, Qiagen) and sequenced using an automated pyrosequencing instrument (PSQ96, Qiagen). The following primer sequences were used for amplification and pyrosequencing of the human and mouse cDNA, respectively:

Human forward PCR primer: 5'-ACAAACCCGTGAAGCATGG

Human reverse PCR primer: 5'Biotin-TACTTCAGGGGGATGAATCTGG

Human pyrosequencing probe: 5'-ATAGGGGCAACACACT

Mouse forward PCR primer: 5'-CCTACAAACCCGTGAAGCA

Mouse reverse PCR primer: 5'Biotin-TTGAGGGGGATGAATCGG

Mouse pyrosequencing probe: 5'-TCGGTGCCACCCACT

Quantitative analysis was performed using Pyrosequencing software from Qiagen.

Western Blot

Western immunoblot analyses were performed to evaluate the protein expression levels of RPS15, RPL5 and TP53. For all assays, a minimum of $5x10^6$ cells were collected, washed with PBS and lysed in RIPA buffer (Sigma #R0278) supplemented with protease and phosphatase inhibitors (Sigma #11836153001 and Sigma #4906845001) for 30 minutes at 4°C. Cell lysate was clarified by centrifugation at 10,000xg for 5 min. Protein concentration was determined using the Pierce bicinchoninic acid assay (Life Technologies #23225) and 40 µg of protein were loaded per lane of a 4-12% Bis-Tris gel (Life Technologies NP0323). Proteins were transferred onto polyvinylidene

fluoride membranes (Life Technologies IB24002) using an iBlot 2 at 20V for 8 minutes and subsequently incubated in 5% BSA, 1X TBST (Teknova #T9511) prior to probing with one of the following primary antibodies (all from Cell Signaling Technology) at a 1:1,000 dilution for 1 hour at room temperature: RPS15 (#PIPA562977, Thermo Fisher Scientific), RPL5 (#14568S, Cell Signaling Technology), TP53 (#9282, Cell Signaling Technology), and GAPDH (#2118). Membranes were washed in TBST prior to incubation with a 1:2000 dilution of goat anti-rabbit HRP-conjugated IgG antibody (Fisher Scientific 12348MI) for 1 hour at room temperature. Membranes were visualized using SuperSignal West Pico Chemiluminescent Substrate (Life Technologies 34580) and quantified using a BioRad ChemiDoc.

Proliferation Assays

Proliferation was measured using the Cell Trace Violet Cell Proliferation Kit and flow cytometry, per the manufacturer's instruction. Dye intensity was determined at baseline and every 24 hours following labeling.

Monitoring of disease in peripheral blood

Mice were monitored monthly from 3 to 24 months of age. Peripheral blood (100 μL) was collected from mice via submandibular bleeds into EDTA-coated tubes. Erythrocyte lysis was performed by incubating blood samples in 1 mL of ACK buffer for 5 min and subsequently washed with PBS supplemented with 2% FCS and 2 mM EDTA. Cells were then stained with a cocktail of antibodies targeting CD5, B220, CD11b, CD3 and IgKappa for 30 mins at 4°C. Cells were then washed and analyzed using flow cytometry.

B cell purification

Mice were euthanized in a CO_2 chamber and spleens or femurs were collected and mechanically dissociated to form a single cell suspension. Erythrocyte lysis was performed using ACK buffer and B cells were immunomagnetically isolated using the MACS Mouse B cell Isolation Kit (Miltenyi Biotec). B cell purity (>90%) was confirmed post-sorting on a FACS Canto I using the flow cytometry staining procedures described above.

Germinal Center Formation

Sheep Red Blood Cells (SRBC,) were spun down at 1200 RPM for 5 minutes, washed with PBS and spun again. Cells were resuspended at a concentration of 6.66x10^9 cells/ml. Mice received 150 ul of SRBC or vehicle (PBS) via IP injection. Ten days post injection, Mice were euthanized in a CO_2 chamber and spleens collected. Spleens were mechanically dissociated. Erythrocyte lysis was performed using ACK buffer and cells were washed with PBS supplemented with 2% FCS and 2 mM EDTA and incubated with the following cocktails of antibodies (all purchased from BioLegend) for 15 minutes at 4ºC. *Cocktail for Germinal Center B cells:* B220-Pacific blue, CD38-APC.Cy7, CD138-PE, CD95-FITC, TACI-APC, for germinal center B cell and Plasma cell quantification. Cells were then washed and analyzed using flow cytometry.

B cell development

Proportions of murine B cell sub-populations at different development stages were determined by flow cytometric analysis of cell surface markers (**Supplemental fig. 4**). Cells were extracted from bone marrow, spleen and the peritoneal cavity and processed as described above (**B cell purification**). Following dissociation and erythrocyte lysis, cells were washed with PBS

supplemented with 2% FCS and 2 mM EDTA and incubated with the following cocktails of antibodies (all purchased from BioLegend) for 15 minutes at 4°C.

Cocktail for splenocyte suspension: CD21-BV421, B220-BV510, CD93-BV650, CD23-BV786, CD38-Alexa647, CD24-Alexa700, CD95-PE, IgD-APC.Cy7 and anti-IgM-PE.Cy7 (for marginal zone B cells, follicular B cells and transitional B cells quantification)

Cocktail for bone marrow suspension: CD43-PE, CD23-BV786, CD24-Alexa700, CD93-BV650, B220-BV421, CD11b-PerCP.C5.5, TER-119-PerCP.C5.5, CD3e PerCP.C5.5, Ly6G/Ly6C PerCP.C5.5, IgD-APC.Cy7 and IgM-PE.Cy7 (for pro-B cells, pre-B cells, immature, transitional and mature B cells quantification)

Cocktail for peritoneal cavity suspension: CD5-APC, B220-BV421, CD43-PE, IgM-PE.Cy7 and CD23-BV786(for B1a cells quantification)

Cells were then washed and analyzed using flow cytometry.

BCR stimulation and Western Blotting

For analysis of BCR signaling transduction, purified splenic B-cells (5 ×10^6) were stimulated in 1ml RPMI 1640 medium (Life Technologies, Woburn, MA) supplemented with 10% FBS, in the presence of 10μg/ml goat anti-mouse IgM (Southern Biotech, Birmingham, AL) for 5 or 15 min at 37°C. Cells were harvested, washed twice with cold phosphate-buffered saline (PBS), spun at 400g for 5 minutes, and cell pellets were frozen at -80C. Prior to western blot analysis cells were thawed on ice and lysed for 30 minutes on ice with RIPA buffer (Boston Bioproducts, Boston, MA) supplemented with a protease inhibitor mix (1 tablet in 10ml RIPA buffer, Roche, San Francisco, CA) and PhosSTOP (1 tablet in 1ml dH_2O at 10X concentration, Roche, San Francisco, CA) . Cell lysate was clarified by centrifugation at 12,000×g for 10 minutes, and cell extracts were collected. Protein concentration was determined using the Pierce bicinchoninic acid assay (Life

Technologies #23225). Then 10 µg of protein were loaded per lane of a 4-12% Bis-Tris gel (Life Technologies NP0323). Proteins were transferred onto polyvinylidene fluoride membranes (Life Technologies IB24002) using an iBlot 2 at 20V for 8 minutes and subsequently incubated in 5% BSA, 1X TBST (Teknova #T9511) prior to probing with one of the following primary antibodies (all from Cell Signaling Technology) at a 1:1,000 dilution overnight at 4°C: RPS15 (#PIPA562977, Thermo Fisher Scientific), rabbit anti-AKT antibody (40D4), anti-p-AKT (Ser473) antibody (D9E), anti-ERK1/2 antibody (137F5), anti-p-ERK1/2 antibody (Tyr202/204) (D13.14.4E), anti-p-SYK (Tyr 525/526), anti-SYK, anti-p-PLCγ1 (Tyr783), anti-PLCγ1 (D9H10) XP, anti-GAPDH (14C10) and polyclonal anti-HSP90. Except RPS15, all antibodies were purchased from Cell Signaling Technology (Danvers, MA). Membranes were washed with 1X TBST (Teknova #T9511) and Horseradish peroxidase-coupled goat anti- rabbit was added (Rockland Immunochemicals Inc, Limerick, PA). The bands were visualized by using the ECL chemiluminescence Western blotting detection system (GE Healthcare, Boston, 824 MA).

Generation of Mouse and Primary Human RNA-sequencing Libraries

Murine B cells ($1x10^6$) were isolated and purified from the spleens of 2-3 month old Rps15 wild-type, heterozygous and homozygous mutant mice (as described above). B220+ CD5+ CLL cells were FACS sorted from human primary CLL samples. Post-isolation, cells were washed in cold PBS and total RNA was extracted using a RNeasy kit (Qiagen). Total RNA was quantified using the Quant-iT RiboGreen RNA Assay Kit and normalized to 5 ng/µL. 2 µL of ERCC controls (using a 1:1000 dilution) were spiked into each sample. For cDNA library preparation, 200 ng per sample was used as input into an automated variant of the Illumina TruSeq Stranded mRNA Sample Preparation Kit (which preserves strand orientation of the RNA transcript). Oligo dT beads were used to enrich mRNA from the total RNA sample, followed by heat fragmentation and cDNA

synthesis. The resultant 400bp cDNA underwent dual-indexed library preparation, including 'A' base addition, adapter ligation using P7 adapters, and PCR enrichment using P5 adapters. After enrichment, libraries were quantified using Quant-iT PicoGreen (1:200 dilution). Samples were subsequently normalized to 5 ng/μL, pooled and quantified using the KAPA Library Quantification Kit for Illumina Sequencing Platforms. The entire process was performed in a 96-well format and all pipetting is executed by either Agilent Bravo or Hamilton Starlet. Samples underwent single-end sequencing for 75 cycles using an Illumina NextSeq platform.

RNA-sequencing Analysis

Patient Samples

RNA-sequencing reads were aligned to the human reference genome GrCH38 using STAR (v2.4.0.1)[52] and TPM (Transcripts Per Kilobase Million) values were used to measure gene expression. Differentially expressed genes were determined using DESeq2[53]. Pathway analysis was performed using the MetaCore software (Clarivate Analytics) or GSEA[54].

Human Cell Lines

RNA-seq reads were aligned with STAR (version 2.5.3a)[52] with the following parameters: --runThreadN 4 --genomeDir /cga/wu/riboseq/reference/STAR_index_RPS15_mCherry --limitBAMsortRAM 30000000000 --outSAMtype BAM SortedByCoordinate --outFilterType BySJout --alignIntronMin 20 --alignIntronMax 100000 --quantMode TranscriptomeSAM --twopassMode Basic. A custom genome was built by adding RPS15 transgene sequences (mutant and wild-type) to the FASTA file of the human genome (hg19). For the transcriptome annotation, a combination of GENCODE v26lift37 transcriptome annotation was combined with transcripts

annotated as tstatus "unannotated" from MiTranscriptome annotation. RSEM (v1.3)[55] was used to quantify transcription against the same transcriptome annotation as above. DESeq2 was used to perform differential gene expression analysis.

Mouse Samples

RNAseq reads were aligned with STAR as described above, except against mouse genome GRCm38 and GENCODE annotation of the transcriptome vM24. Quantification was performed with RSEM. Differential gene expression analysis was performed with DESeq2.

Generation of Human Ribo-seq Libraries

We obtained ribosome-protected footprints and matching mRNA sequencing data for the HG3 RPS15 WT and MT^{S138F} overexpression cell lines +/- TP53 deletion (30 µg RNA per sample, 3 biological replicates per condition). RNA-seq libraries were prepared and sequenced as described above. Ribo-seq libraries were generated as previously described,[56] with several adaptations. Linkers were designed with 12 random nucleotides forming the UMI rather than 5. RNA from unprotected by ribosomes was degraded using a 1:20 dilution of RNaseI and treated for 15 minutes at room temperature. Ribosomes were isolated using a size-exclusion column as described in the Illumina TruSeq Ribo Profile Kit protocol. Ribosome profiling libraries were sequenced with a single-end 50 bp run on a NextSeq500.

Ribo-seq Analysis

Adapter (AGATCGGAAGAGCACACGTCTGAA) was removed using fastx_clipper from FASTX-Toolkit. UMIs were removed using umi_tools. Ribosomal RNA and tRNA were removed

using Bowtie version 1.0.05. Remaining reads were aligned to the genome (hg19 / GRCh37) and transcriptome using STAR (v2.5.3a6) (--alignIntronMin 20 --alignIntronMax 100000 --outFilterMismatchNmax 1 --outFilterType BySJout --outFilterMismatchNoverLmax 0.04 --twopassMode Basic). For the transcriptome annotation, a combination of GENCODE v26lift37 transcriptome annotation was combined with transcripts annotated as tstatus "unannotated" from MiTranscriptome annotation. To determine the RPF library quality, trinucleotide codon periodicity was plotted using RibORF readDist script8 against annotated protein-coding ORFs (GENCODE v26lift37). Ribo-seq reads were quantified at ORF resolution using a custom script rpfTPM available at https://github.com/TamaraO/Riboseq-tools. Differential translation analysis was performed using DESeq2 and deltaTE[57].

Mouse Models

All animals were housed at Dana-Farber Cancer Institute (DFCI). All animal procedures were completed in accordance with the Guidelines for the Care and Use of Laboratory Animals and were approved by the Institutional Animal Care and Use Committees at DFCI. *Rps15*-S138F floxed mice (C57BL/6 background) were generated (Biocytogen, MA) by flanking endogenous WT exons 3, 4 and a stop codon with Lox-P sites followed by exons 3 and 4 with the *RPS15-S138F* point mutation knocked-in to exon 4. In the presence of Cre recombinase, the sequence between the LoxP sites is removed, allowing for the expression of the Rps15 mutant allele. *Trp53*del mice (B6.129P2-Trp53$^{tm1Brn/J}$) were purchased from the Jackson Laboratory. To obtain B cell-specific expression, *Rps15*-S138F floxed mice and *Trp53* floxed mice were crossed with *Cd19*-Cre/Cre mice to generate either *Cd19*-Cre/+ *Rps15* fl/+ (*RPS15*^{het}) or *Cd19*-Cre/+ *Trp53* fl/+ (*Trp53*^{het}) mutant mice. These heterozygous mutant mice were then crossed to generate Rps15 or

Trp53-expressing homozygous mice, which were then crossed to each other to generate *Cd19* Cre/+ *Trp53*fl/+ *Rps15* +/+, fl/+ or fl/fl (WT, heterozygous or homozygous) mice. In all cases, genotypes were confirmed by PCR of tail gDNA using a set of primers targeting the floxed allele:

Rps15 Forward: 5'-GCAAGCGCTCTAGATTGTGACCTC

Rps15 Reverse: 5'-CTCTAAAATGAATCCACCAGCTTCCAC

Trp53 Forward: 5'-GGTTAAACCCAGCTTGACCA

Trp53 Reverse: 5'-GGA GGC AGA GAC AGT TGG AG

Activation of the floxed allele by Cre recombinase was confirmed by PCR on gDNA from purified B cells and non-B cell fractions using a set of primers that amplifies the activated allele:

Cre-activated Forward: 5'-GCAAGCGCTCTAGATTGTGACCTC

Cre-activated Reverse: 5'-GGAGACTGAGGCAGATCTGTCGAC

This reaction amplifies the target activated allele at 142 bp. Presence of the activated allele was only detected in the purified B cell fraction.

Patient samples

Primary CLL samples were obtained from Avicenne Hospital, Assistance Publique-Hôpitaux de Paris, Bobigy, France and from the CLL-1100 project (including patients from the German, Spanish, MD Anderson and DFCI cohorts)[6]. Samples from the CLL-1100 project were collected as previously described[1,6]. For samples from Avicenne Hospital, informed consent was obtained from all subjects and specimens were collected in accordance with the principles of the Declaration of Helsinki and with the approval of the Institutional Review Boards of Avicenne Hospital and Dana-Farber Cancer Institute. Tumor samples were collected upon diagnosis and prior to therapy. Fresh CLL cells were isolated from peripheral blood via Ficoll and flow cytometry analysis

confirmed tumor purity of >80% in all cases. Next-generation sequencing (NGS) was performed on 277 progressive CLL patients (sex ratio M/F: 2.4/1) with a median age of 60.7 years. All blood samples underwent IGHV sequencing for assessment of mutational status, conventional cytogenetics, fluorescence in situ hybridization (FISH) analysis of trisomy 12, 11q, 13q and 17p deletions and amplicon-based NGS sequencing of CLL-related mutated genes (*TP53*, *NOTCH1*, *SF3B1*, *FBXW7*, *RPS15*, *POT1*, *MYD88*, *BIRC3*, *ATM* and *XPO1*).

Statistical analyses

Statistical analysis was performed using GraphPad Prism 7. P-values were calculated using a two-sample Student t-test (after confirming homogeneity of variance) or Mann Whitney test. For comparison of 3 groups, p-values were calculated with a one-way ANOVA test followed by Tukey's multiple comparison test after confirming homogeneity of standard deviation.

2.3 Results

Recurrent *RPS15* mutations in patient samples

Using a compilation of patient data, we have analyzed whole exome sequencing (WES) from over 1,100 patients[25]. From this group we have identified 15 patients with *RPS15* mutations, all of which occur within a 14 amino acid region of exon 4 in the C terminus region of the protein (**Table 1, Fig. 1a**). These findings are consistent with those previously reported in the literature[5,33,36]. All *RPS15* mutated samples had unmutated IGHV, and 3 patients (20%) also had a del(17p), a *TP53* mutation, or both. *RPS15* mutations were designated as clonal in 50% of samples (allelic frequency >35%). For the 11 patients for which we had clinical data, 11 patients eventually required treatment, with 63% relapsing and 55% deaths.

Our group further performed targeted next-generation sequencing (NGS) of a panel of putative CLL drivers (i.e. *RPS15*, *NOTCH1*, *FBXW7*, *POT1*, etc., **Methods**) in a separate cohort of 277 patients with progressive CLL, in order to determine whether *RPS15* mutations co-occur with mutations other than *TP53*. We identified 19 additional mutated cases in this cohort (7.9%), with a median allelic frequency of 38% (average=31.3%) of predominantly *IGHV* unmutated samples (17/19 patients) (**Table 1**). We observed the co-occurrence of *RPS15* mutations with *TP53* mutations in 6 of 19 patients (32%). Of note, 5 of 19 patients (26%) who did not contain *TP53* alterations, had mutations in DNA-damage associated genes such as *ATM* and *POT1*, making the case for the possible role for loss of DNA repair pathways in *RPS15*-mutated CLL.

Consistent with previous data, *RPS15* mutations in the discovery and validation cohorts predominantly were identified in a region spanning amino acids 129-145, with the highest rate of mutations occurring in residues 131, 136 and 138 (**Fig. 1a**). This region has previously been

described to interact with the A and P decoding sites of the ribosome, with likely effects on translation and ribosome stability[58,59].

Figure 1

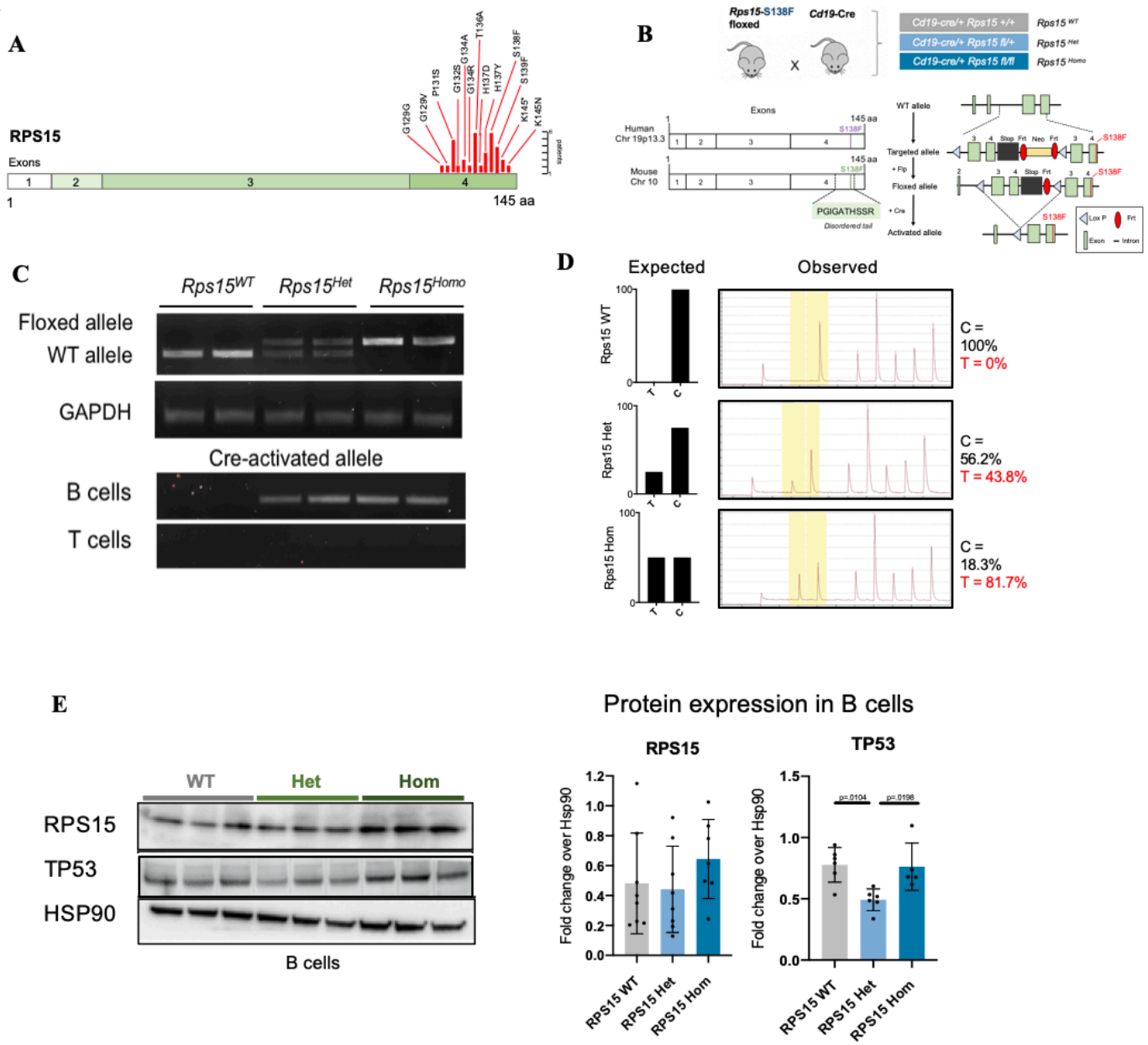

F

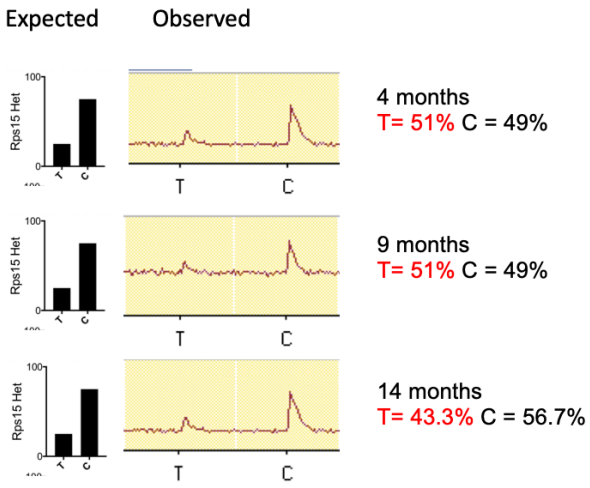

Figure 1 **Generations and validation of mouse model with B-cell specific expression of *Rps15*-S138F allele.**
(a) Schematic of localization of *RPS15* mutations as observed in CLL patients.
(b) Schema of the strategy for generating mouse model with B-cell specific expression of *Rps15*-S138F allele.
(c) Presence of the activated *Rps15*-S138F allele was restricted to B cells as detected by PCR of gDNA
(d) Expression of MT and WT alleles in purified mouse B splenocytes were detected by pyrosequencing of amplified cDNA. Left, expected pyrograms; right, observed pyrograms, with *Rps15* MT transcript ratio relative to the WT transcript in *Rps15*^{WT}, *RPS15*^{het} and *RPS15*^{hom} mice.
(e) Western blot analysis of RPS15 and TP53 protein levels in *Rps15*^{WT}, *RPS15*^{het} and *RPS15*^{hom} mice. HSP90 used as loading control
(f) Expression of MT and WT alleles in purified mouse B splenocytes across different age groups were detected by pyrosequencing of amplified cDNA. Left, expected pyrograms; right, observed pyrograms, with *Rps15* MT transcript ratio relative to the WT transcript *RPS15*^{het} mice at 4, 9 and 14 months of age.

***RPS15* mutation impacts B cell development and proliferation**

To interrogate the impact of *RPS15* mutation on B cell function, our group generated a mouse model with conditional expression of the most commonly occurring *RPS15*-S138F mutation in CLL (**Fig. 1b**). B cell-specific expression was achieved by crossing a mouse line carrying a floxed *Rps15*-S138F (*RPS15*$^{fl/+}$) allele with homozygous *Cd19*-Cre (*Cd19*-Cre$^{+/+}$) mice, yielding WT (*Cd19*-Cre$^{+/-}$ *Rps15*$^{+/}$, *RPS15*^{WT}), heterozygous (*Cd19*-Cre$^{+/-}$ *Rps15*$^{fl/+}$, *RPS15*^{Het}) and homozygous (*Cd19*-Cre$^{+/-}$ *Rps15*$^{fl/f}$, *RPS15*^{Hom}) MT mice (**Fig.1b**, top). The presence of the floxed allele was confirmed by targeted PCR of genomic DNA (gDNA) and Cre-mediated activation of the MT allele specifically in CD19^{+} splenic B cells (**Fig. 1c**). Targeted allele-specific quantitative RNA sequencing (RNA-seq) by pyrosequencing revealed that the MT allele was stably detected (**Fig. 1d**) as expected in both heterozygous and homozygous mice. In heterozygous mice the mutant allele was expressed at 56%, while in homozygous mice the mutant allele was expressed at 81%. These findings in homozygous mice may be explained by imperfect excision of loxP sites in homozygous mice.

Quantification of protein from murine B cells by western blot revealed that *RPS15*^{Hom} B cells expressed RPS15 protein at slightly higher levels than *RPS15*^{Het} and *RPS15*^{WT} mice **(Fig. 1d,** right), perhaps indicating a compensatory mechanism against dysfunctional RPS15 activity. However, across genotypes RPS15 protein levels were variable between individual mice, indicating possible variability of RPS15 levels within the murine population. Protein levels of TP53 from *RPS15*^{Het} mice was significantly decreased compared to *RPS15*^{WT} and *RPS15*^{Hom} mice (**Fig.1e**, left). This may be due to the impact of RPS15 as a regulator or p53 stability. Additionally, we used targeted allele-specific quantitative RNA-seq by pyrosequencing revealed that the MT allele was stably detected across the lifespan of the mice (**Fig. 1f**). The MT allele was detected at

consistent levels across 4-, 9- and 14-month *RPS15*^{Het} mice. Consistent with observations by our group that *RPS15* MT-overexpressing human B cells exhibit proliferation deficits, we observed that the proportion of murine B cells comprising the circulating lymphocytes in peripheral blood was reduced by ~50% in *RPS15*^{Hom} mice as compared to *RPS15*^{Het} and *RPS15*^{WT} mice across all the mouse life span, up to 15-18 months when reductions were seen across all genotypes (**Fig. 2a**).

In order to see the impact of *RPS15* mutation of the development of B cells *in vivo* we assessed B-cell subpopulations in the bone marrow, spleen and peritoneal cavity in young mice (3 months old) by multi-parameter flow cytometry (**Fig 2b-e**). To assess the proportions of B cell subsets, we followed the gating strategy and analyzed subpopulations outlined in Lazarian et. al 2021 (**Supplemental Fig. 4**)[2].

B cell development begins in the fetal liver, and fetal/ adult bone marrow, where it eventually enters circulation and completes maturation in secondary lymphoid tissues, such as lymph nodes or spleen[60]. During B cell development B cells are characterized by a number of surface markers as well as the stage of rearrangement of their Ig receptor. B cells originate from the common lymphoid progenitor (CLP) where B cell fate is determined, this is followed by rearrangement of the heavy (IgH) and light chain (IgL) loci. In the first stage of development pro-B cells rearrangement of the IgH locus begins, initiating the transition into pre-B cells. In between these stages, the B- lymphocyte surface antigen (CD19) starts to be expressed. Its expression continues to increase during the maturation of B cells[61]. Within our model, expression of the MT-allele follows the advent of CD19 expression, therefore we would expect impacts from the mutant allele to influence late stage B cells rather than the populations in early development. Further maturation leads to transitional B cells which have co-expression of the μ (IgM) and δ (IgD) heavy chains, and cells begin to leave the bone marrow and enter secondary lymphoid tissue.

In a comparison of B cell development sub-populations, we looked at changes in early (CD34+) and late stage (CD34-) B cell development in the bone marrow. There was little change seen between genotypes in the total quantification of late stage B cells (**Fig. 2a**, right). Looking more closely within the subpopulations of B cell progenitors within the late stage (CD34-) B cell population, we identified an increase in immature B cells, followed by decrease in transitional B cells in the *RPS15*^{Hom} mice (**Fig 2c**). This may further implicate developmental block in homozygous *Rps15* MT B cells.

We observed a drastic decrease in marginal zone B cells (B220+ CD21^{high} CD23-) within the splenic B cell population of *RPS15*^{Het} mice as compared to and *RPS15*^{WT} (p=.029). However, *RPS15*^{Hom} saw a marked increase in marginal zone B cells as compared to both *RPS15*^{WT} (p=.0049) and *RPS15*^{Het} (p<.0001) (**Fig. 2d**, left). There appeared to be compensatory decrease of follicular B cells (B220+ CD21- CD23^{high}) of *RPS15*^{Hom} mice compared to *RPS15*^{Het} (p= .0124) and *RPS15*^{WT} (p=.0539) (**Fig. 2d**, right). These findings suggest that *RPS15* mutations influence cell fate within the mature B cell population. There were no significant changes observed between T1 and T2 cell subpopulations across the three genotypes. We observed a significant decrease in B1a (B220+ CD5^{high}) cells within the peritoneal cavity of *RPS15*^{Het} mice as compared to *RPS15*^{WT} (p=.0062) and an even further decrease in *RPS15*^{Hom} mice compared to *RPS15*^{WT} (p<.0001) (**Fig. 2e**, left). However, there were no changes in B1b (B220+ CD5^{low}) cells across the different genotypes (**Fig 2f,** left).

As we have shown that *RPS15* mutations impact cell survival and cell fate, we predicted that mutant cells would have impaired immune response capabilities. During a T-dependent antigen response, B cells undergo large amounts of proliferation to drive germinal center

formation, where B cells further divide, undergoing affinity maturation and somatic hypermutation[62]. Together, these steps help generate an adaptive immune response for highly specific antibodies against a pathogen. In order to test the impact of *RPS15* mutations on the immune function of B cells, we looked at their ability to form germinal centers. We injected 3-month-old mice with the T-cell dependent antigen sheep red blood cells (SRBC) or PBS (control) via IP injection. After 10 days splenocytes were collected and germinal center B cells (B220+ CD95+ CD38-) were quantified by flow. We saw no germinal center formation within mice that received the PBS injections (**Fig. 2f**). In mice injected with SRBCs, we saw a significant decrease in germinal center formation in *RPS15*^{Het} (p=.013) and a slight decrease in *RPS15*^{Hom} mice. These findings, indicate that the presence of *RPS15* mutations impair B cell function as an adaptive immune cell.

One of the major determinants of marginal zone versus follicular B cell fate is the strength of BCR signaling[63]. Following our results demonstrating changes in the amount MZ B cells across the different genotypes, we looked into how changes to BCR signaling may be impacting these results. In order to understand how *RPS15* mutations alter BCR signal transduction we stimulated murine B cells with anti-IgM antibodies for 5 and 15 minutes. Following stimulation cells were lysed and phospo- and total protein was measured by western blot. We saw no change in phosphorylation patterns in early signaling proteins (SYK, AKT and PLCγ) across all three *RPS15* genotypes (**Fig. 2g**). Interestingly, we saw a sustained phosphorylation of ERK in *RPS15*^{Het} and *RPS15*^{Hom} mice. In *RPS15*^{WT} we observed a decrease in the ratio of phosphorylated to total ERK protein after 15 minutes of anti-IgM stimulation, while we saw continued levels of increased phosphorylation at this time point in *RPS15*^{Het} and *RPS15*^{Hom} B cells. This finding was of note,

due to the relation of ERK to MYC in the BCR signaling cascade (**Fig. 2g**, top left) since Myc targets have been implicated as a dysregulated pathway in a number of different cancers.

The BCR-associated tyrosine kinase, ZAP70, has been recently associated could directly influence Myc levels and promote cell survival independent of a BCR signal[64]. We found that there was an increase in the baseline levels of ZAP70 protein expression in *RPS15*^{Hom} versus *RPS15*^{Het} (p=0.067) and *RPS15*^{WT} (p=.032) murine B cells (**Fig. 2h**) These results indicate that altered expression of ZAP70 levels may be one mechanism by which *RPS15* mutations mediate MYC activity and thus cell survival even in the absence of a BCR signal.

Figure 2

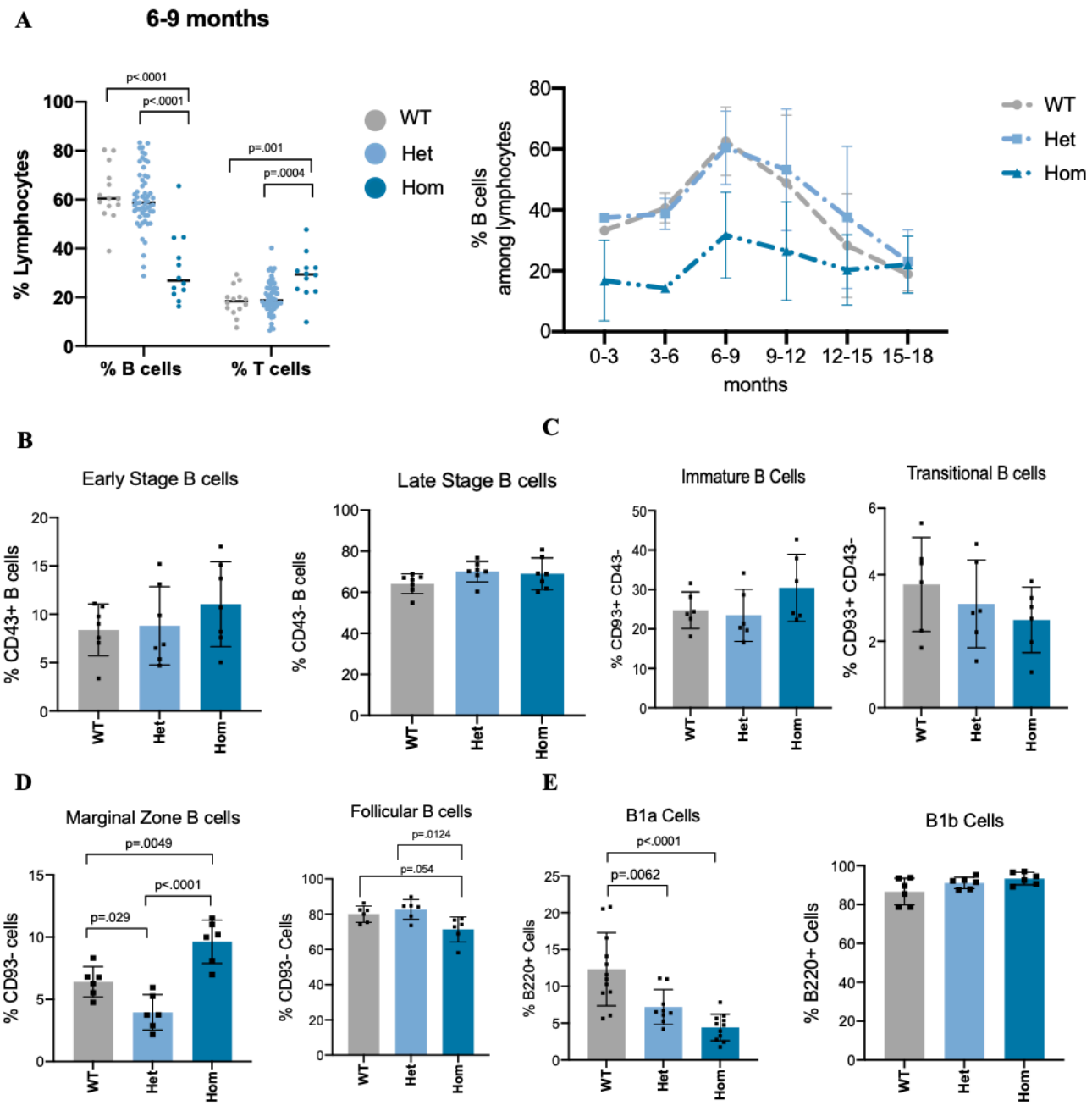
A
6-9 months
p<.0001
p<.0001
p=.001
p=.0004
% Lymphocytes
% B cells
% T cells
WT
Het
Hom
% B cells among lymphocytes
0-3
3-6
6-9
9-12
12-15
15-18
months
B
Early Stage B cells
% CD43+ B cells
Late Stage B cells
% CD43- B cells
C
Immature B Cells
% CD93+ CD43-
Transitional B cells
% CD93+ CD43-
D
Marginal Zone B cells
p=.0049
p<.0001
p=.029
% CD93- cells
Follicular B cells
p=.0124
p=.054
% CD93- Cells
E
B1a Cells
p<.0001
p=.0062
% B220+ Cells
B1b Cells
% B220+ Cells

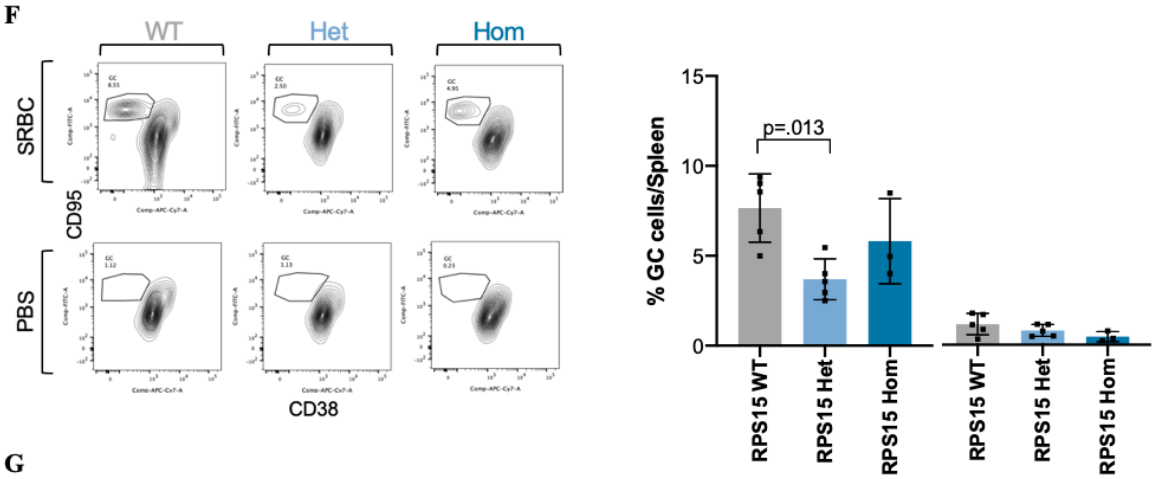
F
WT
Het
Hom
SRBC
PBS
CD95
CD38
% GC cells/Spleen
p=.013
RPS15 WT
RPS15 Het
RPS15 Hom
RPS15 WT
RPS15 Het
RPS15 Hom

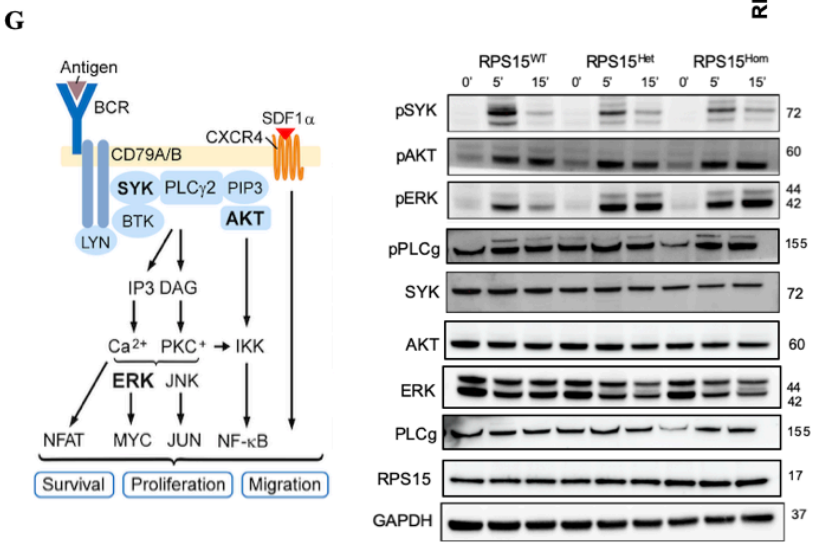
G
Antigen
BCR
SDF1α
CXCR4
CD79A/B
SYK
PLCγ2
PIP3
BTK
AKT
LYN
IP3 DAG
Ca2+
PKC+
IKK
ERK
JNK
NFAT
MYC
JUN
NF-κB
Survival
Proliferation
Migration
RPS15WT
RPS15Het
RPS15Hom
pSYK
pAKT
pERK
pPLCg
SYK
AKT
ERK
PLCg
RPS15
GAPDH

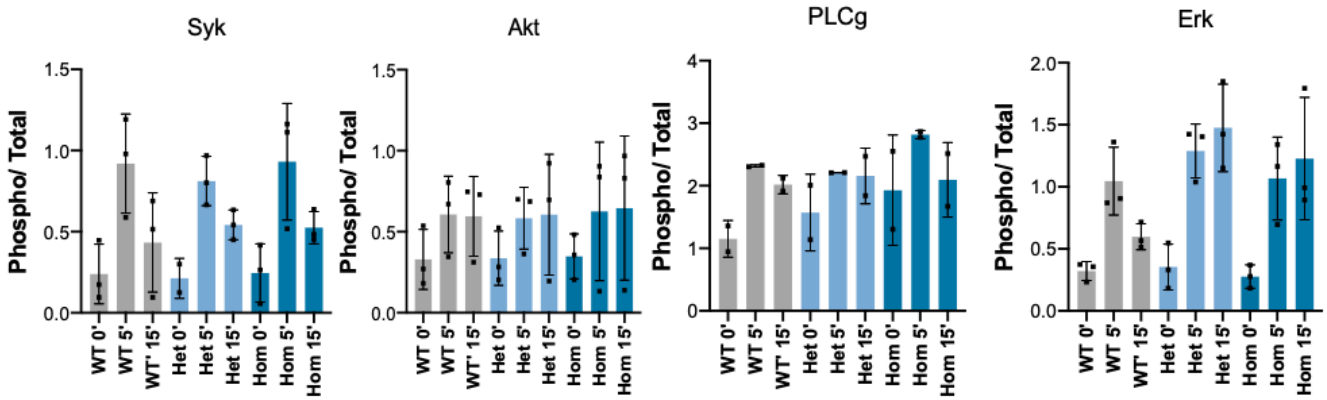
Syk
Akt
PLCg
Erk
Phospho/ Total
WT 0'
WT 5'
WT' 15'
Het 0'
Het 5'
Het 15'
Hom 0'
Hom 5'
Hom 15'

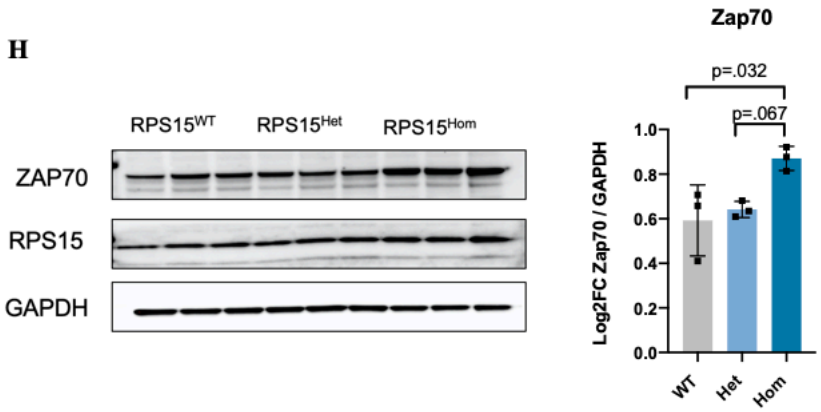

Figure 2 ***RPS15* mutation affects B cell development, proliferation and function.**
(a) Proportion of B cells comprising lymphocyte population of peripheral blood in *RPS15*^{WT}, *RPS15*^{het} and *RPS15*^{hom} mice. Left, 6-9 months of age; Right, Across all ages.
(b) Percentages of early stage or late stage B cells present in bone marrow of *RPS15*^{WT}, *RPS15*^{het} and *RPS15*^{hom} mice (n=6).
(c) Percentages of transitional B cells present in bone marrow of *RPS15*^{WT}, *RPS15*^{het} and *RPS15*^{hom} mice (n=6). Data represent Mean±SEM and were compared using one-way ANOVA followed by Tukey's multiple comparison test.
(d) Percentages of marginal zone or follicular stage B cells present in spleen of *RPS15*^{WT}, *RPS15*^{het} and *RPS15*^{hom} mice (n=6). Data represent Mean±SEM and were compared using one-way ANOVA followed by Tukey's multiple comparison test.
(e) Percentages of B1a and B1b cells present in peritoneum of *Rps15*^{WT}, *RPS15*^{het} and *RPS15*^{hom} mice (B1a, n=12) (B1b, n=6). Data represent Mean±SEM and were compared using one-way ANOVA followed by Tukey's multiple comparison test.
(f) Right, FACS plot analysis of germinal center B cells (GC) from the total splenocytes suspension 10 days after immunization with sheep red blood cells (SRBC) or with the vehicle (Phosphate-buffered saline, PBS)
Left, the percentage of GC B cells, identified as B220, CD95 positive, CD38 negative, isolated from spleen 10 days after immunization with SRBC or with the vehicle (PBS). Data represent Mean±SEM and were compared using one-way ANOVA followed by Tukey's multiple comparison test.
(g)Top right, BCR signaling pathway diagram. Top left, Representative Western Blot of BCR signaling components in splenic B cells 0, 5, 15 minutes following BCR stimulation with anti-IgM. Bottom, Quantified data using ImageJ Mean±SEM of phosphor/total protein and data compared using one-way ANOVA followed by Tukey's multiple comparison test.
(h) Left, Western Blot of Zap70 in splenic B cells from *RPS15*^{WT}, *RPS15*^{het} and *RPS15*^{hom} mice. Right, Quantified data using ImageJ Mean±SEM of total ZAP70 protein/ GAPDH and data compared using one-way ANOVA followed by Tukey's multiple comparison test.

***RPS15* mutations drive CLL-like disease in mice**

In order to determine whether *Rps15* mutation alone or in combination with *Trp53* deletion can lead to CLL-like disease, we established four cohorts of 40 mice each (i.e. RPS15^{WT}, *RPS15*^{MT}, *Trp53*^{MT} and *RPS15*^{MT}/*Trp53*^{MT} [DM] mice). We observed the presence CLL-like cells (B220^{+}CD5^{+}) in the *RPS15*^{MT}, *Trp53*^{MT} and *RPS15*^{MT}/*Trp53*^{MT} mice. Additionally, enlarged spleen observe in *Trp53*^{MT} and *RPS15*^{MT}/*Trp53*^{MT} groups. These were further confirmed by IHC staining of peripheral blood smears (**Fig. 3a**). To follow the acquisition and progression of CLL within the observation cohort, monitored peripheral blood for the appearance of B220^{+}CD5^{+} cells for up to 24 months of age (**Fig. 3c**). At 24 months or end of life we monitored mice for B220^{+}CD5^{+} cells by flow cytometry in peripheral blood, spleen, peritoneal cavity and bone marrow. Of the 10 mice that developed CLL like disease within the *RPS15*^{MT} cohort, we observed the highest levels of B220^{+}CD5^{+} cell infiltration within the peritoneal cavity making up an average of 68.33% of lymphocytes, followed by 32.97% in the blood, 20.13% in the spleen and 4.5% in the bone marrow (**Fig. 3b**). This may indicate an introduction of CLL-like cells in the peritoneum followed by the metastases of cells to the other organs in the same order as the progression of infiltration. In 2 of 30 TP53 MT mice (aged 17 – 20 months), we identified circulating disease, in 3 we observed an enlarged spleen without evidence of circulating disease and 1 mousse with a solid mass (**Fig. 3c**). The levels of CLL in *Trp53*^{MT} were far lower than those observed in RPS15 MT and DM mice. IHC staining of peripheral blood showed the presence of large, binucleated nuclei and was deemed an aggressive, high-grade lymphoma by pathologists (**Fig. 3a**).

In 5 of 40 RPS15^{MT} mice (aged 16 – 22 months), we identified solid, non-lymphoid masses without evidence of circulating disease (H&E staining of these masses are currently underway)

(**Fig. 3c**). Within the *RPS1* ^{MT} we detected B220^{+}CD5^{+} CLL-like cells within peripheral blood mononuclear cells starting from 21 months of age in 10 of the *RPS15*^{MT} mice, with the percentage of circulating B220^{+}CD5^{+} cells rising between 20% and 75% by 24 months of age (**Fig. 3c**). In the DM mice, we detected B220^{+}CD5^{+} CLL-like cells starting from 15 months of age in one of the DM mice (**Fig. 3c**), with the percentage of circulating B220^{+}CD5^{+} cells rising to 90% by 18 months of age. In both *RPS15*^{MT} and DM cohorts, there was evidence of bone marrow, spleen, and peritoneal cavity involvement consistent with CLL-like disease. This was further confirmed by IHC staining of tissue from mice with CLL like disease (**Fig 3d**). In *RPS15*^{MT} mice IHC staining of spleen demonstrated infiltration with small lymphocytes, occasional PAX5/CD5 double positive cells are present, with no overt features of large cell transformation. In the BM discretely infiltrated, PAX5/CD5 double positive cells in small aggregates were present (**Fig. 3d**). In *RPS15*^{MT}/*Trp53*^{MT} we observed infiltration with small to medium sized lymphocytes, PAX5/CD5 double positive cells. Overall morphology consistent with features of CLL, potentially some large cell features in the spleen. In the BM, we saw infiltration with small to medium sized lymphocytes in sheets, PAX5^{dim}/CD5+ (**Fig. 3d**). Interestingly, we also observed infiltration within the liver of *RPS15*^{MT}/*Trp53*^{MT} mice with CLL. These findings are an early indication that *Rps15* mutation can drive CLL development in mice, and that co-mutation with *Trp53* alters the aggressiveness and morphology of CLL-like disease, similar to observations in patients[1]. Consistent with patient data, where 32 out of 34 patients had unmutated IGHV (**Table 1**), NGS analysis of BCRs showed that all mice that developed CLL- like disease had unmutated IGHV segments (**Supplementary Table 1**).

Figure 3

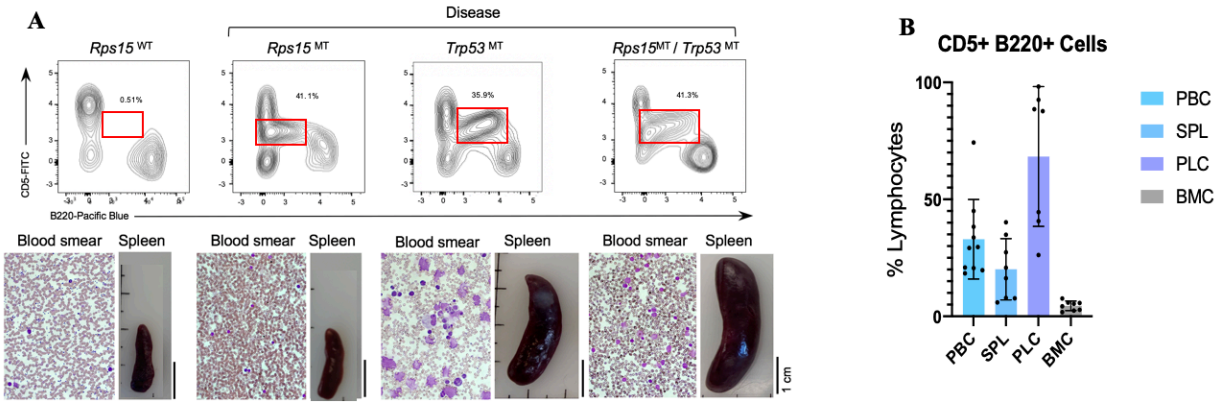

	*Rps15*WT	Rps15MT	Trp53MT	Rps15MT/Trp53MT
	40	**40**	**40**	**40**
CLL	0	10	3	5
Other Lymphoma	0	0	4	0
Solid Masses	0	5	1	1

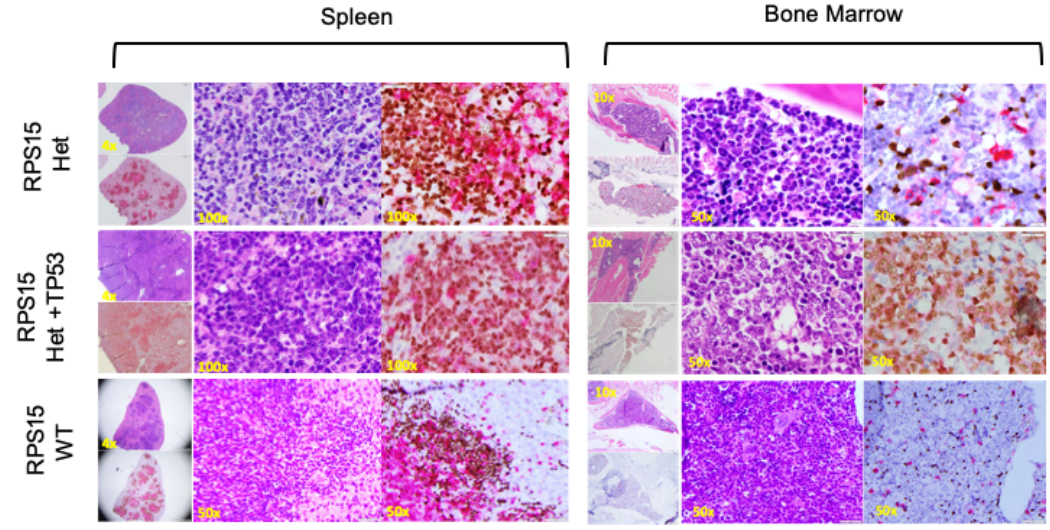

Figure 3 ***RPS15* and *TP53* mutations drive CLL development.**
(a) Top, percentage of CLL cells in peripheral blood by flow cytometry of CLL mice. Bottom, blood smears and spleens of mice with and without CLL.
(b) Detection of B220+ CD5+ cells in peripheral blood, spleen, bone marrow and peritoneum of RPS15 Het mice with CLL by flow cytometry.
(c) Detection of B220+ CD5+ cells in peripheral blood over time. Table, number of cases of CLL, other lymphoma, or solid masses across genotypes.
(d) HE staining and immunohistochemical staining of CD5+PAX5+ cells in the spleen and bone marrow of RPS15 Het- CLL, RPS15 Het TP53 Het- CLL, and RPS15 WT mice at 4X, 50X and 100X zoom.

RPS15 mutations alter cMyc signaling

RPS15 mutations localize to an evolutionary conserved region of the gene that when expressed, interfaces with the mRNA decoding site of the ribosome and likely plays a role in mRNA translation[59]. We thus sought to characterize the impact of *RPS15* mutation on transcription and translation. We performed RNA-seq analysis on purified splenic B cells from 3-month old $RPS15^{WT}$, $RPS15^{het}$ and $RPS15^{hom}$ mice (n=3 per cohort). Altogether, we identified a total of 364 and 1,232 significantly upregulated and 835 and 1,181 significantly downregulated genes in the $RPS15^{MT}$ vs $RPS15^{WT}$ mice ($RPS15^{het}$ and $RPS15^{hom}$, respectively) (**Fig. 4a**, log2FC >0.3, p<0.05). Gene set enrichment analysis (GSEA) of these differentially expressed signatures revealed a strong enrichment for MYC target genes in $RPS15^{Hom}$ vs $RPS15^{WT}$, appearing at the top most upregulated pathway (**Fig. 4b**). Findings from GSEA analysis also demonstrated a strong downregulation of MYC target genes in $RPS15^{Het}$ vs $RPS15^{WT}$ (**Fig. 4c**) and was identified as the most downregulated pathway. Findings of upregulation of MYC targets in $RPS15^{Hom}$ B cells is consistent with GSEA analysis of RNA-seq data from the HG3 *RPS15* mutant overexpression cell lines (MT vs WT +/- *TP53* deletion) and of primary, untreated samples from 3 CLL patients with *RPS15* mutation (as compared to 3 *RPS15* WT CLL samples of similar genetic background) (**Fig. 4e)**. ~3-5% of differentially expressed genes (*RPS15* MT vs WT) were shared between the HG3 line, mouse

model and primary patient samples (**Fig. 4d**, log2FC>0.5, p<0.1), many of which were involved in transcription and translation (i.e. *MED23*, *POLM*, *POLR1A*, *EDC4*, *MRPL55*, etc.). Reactome pathway analysis of these differentially expressed signatures across all four models revealed a common enrichment in translational machinery, such as mRNA splicing and processing, rRNA processing and modification, snRNP assembly, and N-glycosylation of protein (**Fig. 4e**, right **normalized** enrichment score>1, nominal p-value <0.05). Although further validation is needed, we hypothesize that *RPS15* mutation induces MYC activation, which in turn increases the transcription of core genes involved in mRNA processing, ribosome biosynthesis and translation – potentially setting the stage for oncogenesis.

Confirmation of RNAseq finding was previously demonstrated by our group by ribosome profiling on the HG3 *RPS15* WT and MT overexpression cell lines (+/- *TP53* deletion)[29]. This technique enabled us to measure translation efficiency (TE) by comparing levels of ribosome-associated mRNA (ribosome footprints) against the total mRNA levels present for each gene. These findings indicated that *RPS15* mutation largely has effects on translation of protein-coding mRNA. Indeed, 3,391 genes were identified with differential TE between *RPS15*-MT vs WT cells, of which 1,754 genes had increased and 1,554 genes had decreased TE (log2FC >0.5, p<0.1). This dysregulation was even more marked in *TP53* KO cells, where we identified 5,499 genes with differential TE between RPS15-MT vs WT cells, of which 1,820 genes had increased and 1,560 genes had decreased TE.

GSEA analysis of genes that are differentially translated in *RPS15* MT- vs WT-overexpressing cells and observed a strong enrichment of *TP53*-related genes (**Fig. 4f,g**), consistent with the activation of stress pathways by *RPS15* mutant expression. In *TP53*-deleted cells, however, we once more observed a strong increase in TE of MYC target genes and of

components of the ribosomal machinery (**Fig. 4f,g**). These findings indicate while *RPS15* mutations set the stage for oncogenesis through dysregulation of MYC targets, the presence of additional mutations, such as in cell cycle regulator genes like *Trp53*, further drive dysregulation and protentional for clonal expansion and oncogenesis.

RNA-seq analysis of murine *RPS15*^{Het} CLL cells vs age-matched of *RPS15*^{WT} B cells revealed a large number of significantly up- and down regulated genes in CLL samples. Identifying 3,171 significantly upregulated and 3,042 downregulated genes (**Fig. 4h**). GSEA of these differentially expressed signatures revealed a strong enrichment for MYC target genes in *RPS15*^{Het} CLL vs *RPS15*^{WT} age matched B cells (**Fig. 4i**). Myc gene targets were the top two upregulated gene pathways identified (Fig. 4J). This indicates a reversal in the transcription regulation of Myc target genes throughout the lifetime, or due to the acquisition of CLL in *RPS15*^{Het} mice. This further supports the hypothesis that the presence of additional mutations leads to cell pathway dysregulation and oncogenesis in cells with *Rps15* mutations. Further analysis comparing age matched *RPS15*^{Het} B cells compared to CLL cells will be necessary to understand the impact of age on transcription in *RPS15*^{Het} mice.

Figure 4

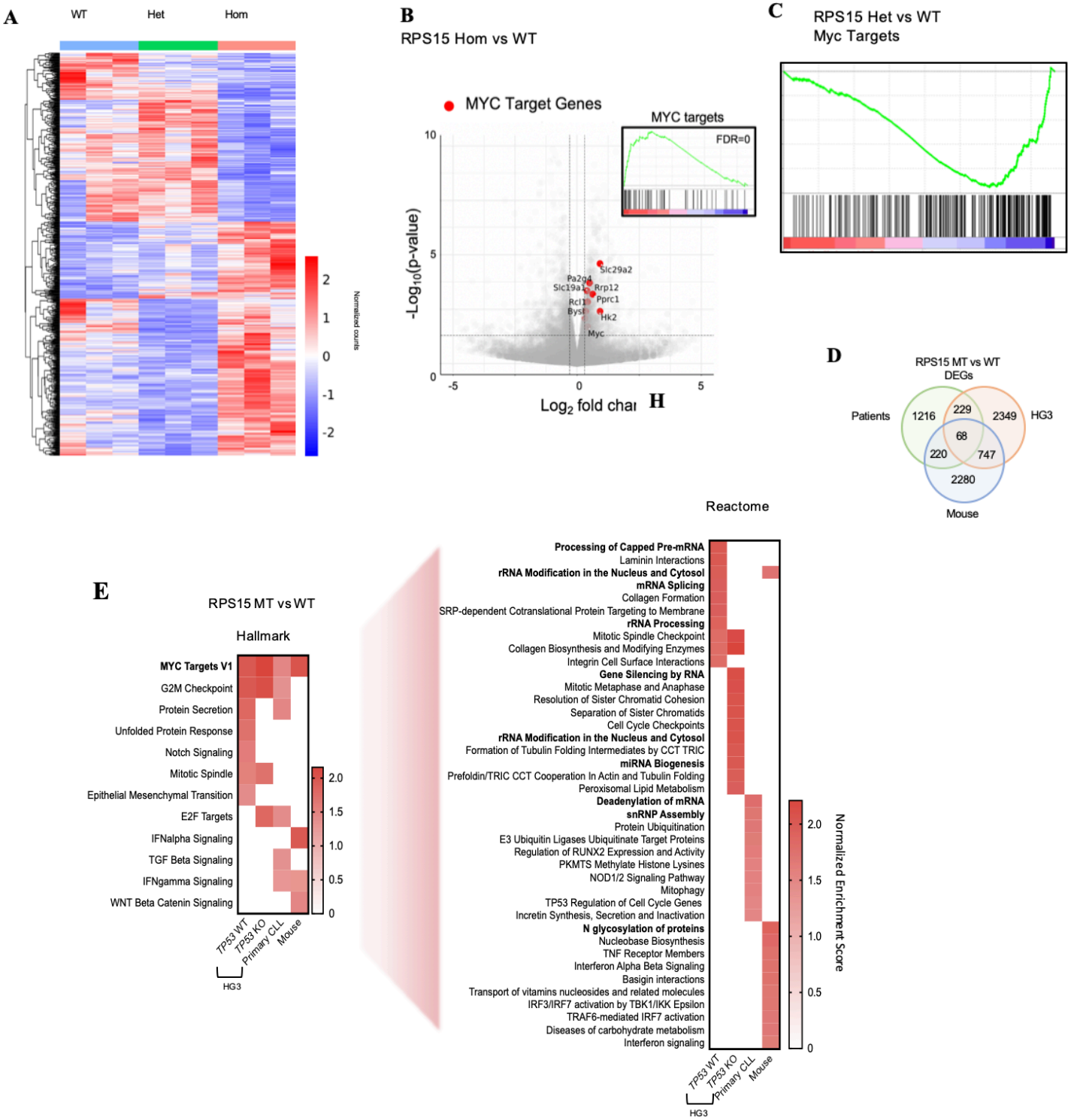
A
WT
Het
Hom
Normalized counts
B
RPS15 Hom vs WT
MYC Target Genes
MYC targets
FDR=0
-Log10(p-value)
Slc29a2
Pa2g4
Slc19a1
Rrp12
Pprc1
Rcl1
Byst
Hk2
Myc
Log2 fold chai
C
RPS15 Het vs WT
Myc Targets
D
RPS15 MT vs WT
DEGs
Patients
HG3
Mouse
1216
229
2349
68
220
747
2280
E
RPS15 MT vs WT
Hallmark
MYC Targets V1
G2M Checkpoint
Protein Secretion
Unfolded Protein Response
Notch Signaling
Mitotic Spindle
Epithelial Mesenchymal Transition
E2F Targets
IFNalpha Signaling
TGF Beta Signaling
IFNgamma Signaling
WNT Beta Catenin Signaling
TP53 WT
TP53 KO
Primary CLL
Mouse
HG3
Reactome
Processing of Capped Pre-mRNA
Laminin Interactions
rRNA Modification in the Nucleus and Cytosol
mRNA Splicing
Collagen Formation
SRP-dependent Cotranslational Protein Targeting to Membrane
rRNA Processing
Mitotic Spindle Checkpoint
Collagen Biosynthesis and Modifying Enzymes
Integrin Cell Surface Interactions
Gene Silencing by RNA
Mitotic Metaphase and Anaphase
Resolution of Sister Chromatid Cohesion
Separation of Sister Chromatids
Cell Cycle Checkpoints
rRNA Modification in the Nucleus and Cytosol
Formation of Tubulin Folding Intermediates by CCT TRIC
miRNA Biogenesis
Prefoldin/TRIC CCT Cooperation In Actin and Tubulin Folding
Peroxisomal Lipid Metabolism
Deadenylation of mRNA
snRNP Assembly
Protein Ubiquitination
E3 Ubiquitin Ligases Ubiquitinate Target Proteins
Regulation of RUNX2 Expression and Activity
PKMTS Methylate Histone Lysines
NOD1/2 Signaling Pathway
Mitophagy
TP53 Regulation of Cell Cycle Genes
Incretin Synthesis, Secretion and Inactivation
N glycosylation of proteins
Nucleobase Biosynthesis
TNF Receptor Members
Interferon Alpha Beta Signaling
Basigin interactions
Transport of vitamins nucleosides and related molecules
IRF3/IRF7 activation by TBK1/IKK Epsilon
TRAF6-mediated IRF7 activation
Diseases of carbohydrate metabolism
Interferon signaling
Normalized Enrichment Score

F

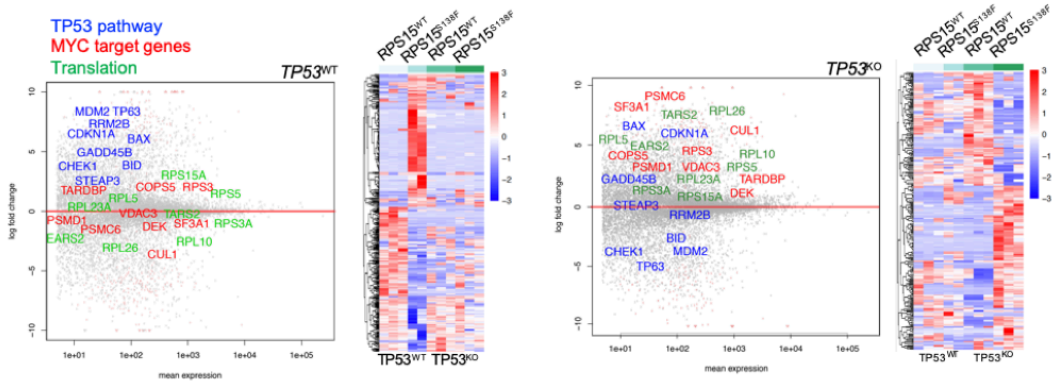
TP53 pathway
MYC target genes
Translation
TP53WT
TP53KO
log fold change
mean expression
RPS15WT
RPS15S138F
TP53WT TP53KO

G

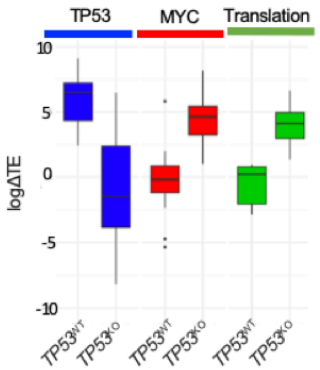
TP53
MYC
Translation
logΔTE
TP53WT
TP53KO

H

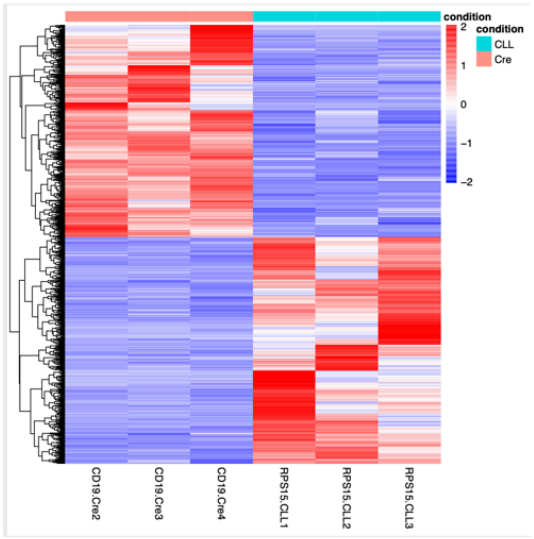
condition
CLL
Cre
CD19.Cre2
CD19.Cre3
CD19.Cre4
RPS15.CLL1
RPS15.CLL2
RPS15.CLL3

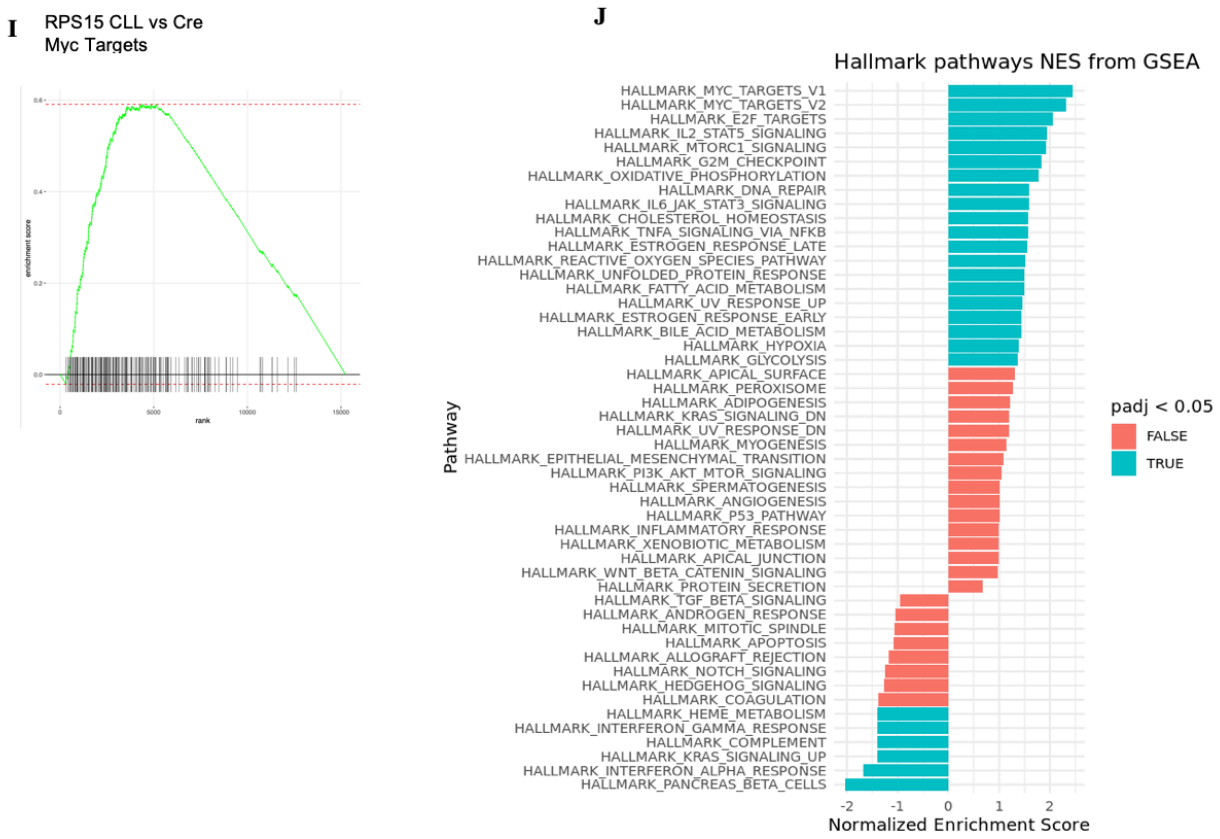

Figure 4 ***RPS15* Mutations drive dysregulation through Myc signaling pathways**
(a) Heatmap showing normalized expression of top dysregulated genes in purified B splenocytes from *RPS15*^{WT}, *RPS15*^{het} and *RPS15*^{hom} mice (3 mice per condition, 3 months of age).
(b) GSEA analysis of *RPS15*^{hom} vs *Rps15*^{WT} mice reveals MYC targets as the top upregulated differentially expressed pathway. Volcano plot displays elevated expression of MYC target genes in *RPS15*^{hom} B cells (log2FC>0.3, p<0.05).
(c) GSEA analysis of *RPS15*^{het} vs *Rps15*^{WT} mice reveals MYC targets as the top downregulated differentially expressed pathway.
(d) Venn diagram of differentially expressed genes (log2FC>0.5, p<0.1) in *RPS15* MT vs WT HG3 cell lines, primary CLL samples (3 *RPS15*^{MT} vs 3 *RPS15*^{WT} CLL patient samples controlled for genetic background and *IGHV* mutation status), and 3 *RPS15*^{HOM} vs 3 *RPS15*^{WT} murine B cells.
(e) Left; GSEA analysis using the Hallmark gene set also reveals MYC as the top differentially expressed pathway in HG3 cell lines (+/- *TP53* KO) and in primary CLL samples. Right; GSEA analysis using Reactome gene set reveals many MYC target genes to comprise top mRNA and rRNA processing pathways. NES>1, normalized p value<0.05.
(f) MA plot and heatmaps of all genes with differential translation efficiency in *RPS15*^{S138F} vs *RPS15*^{WT} overexpression cell lines. Left = *TP53*^{WT}; Right = *TP53*^{KO}. (blue = *TP53* pathway, red = MYC targets, green = translation).

(g) Box plot of differential translation efficiency values for *RPS15*^{S138F} vs *RPS15*^{WT} (*TP53* WT or *TP53* KO) showing mean, IQR, range and outliers across gene sets (blue = *TP53* pathway, red = MYC targets, green = translation).
(h) Heatmap showing normalized expression of top dysregulated genes in purified CLL cells from *Rps15*^{Het}, vs age matched *RPS15*^{WT} B cells (3 mice per condition, 21-24 months of age).
(i) GSEA analysis of murine *RPS15* CLL vs *RPS15*^{WT} B cells reveals MYC targets as the top upregulated differentially expressed pathway.
(j) GSEA analysis using the Hallmark gene set also reveals MYC as the top differentially expressed pathway in HG3 cell lines (+/- *TP53* KO) and in primary CLL samples. Right; GSEA analysis using Reactome gene set reveals many MYC target genes to comprise top mRNA and rRNA processing pathways. NES>1, normalized p value<0.05.

2.4 Discussion

Across a number of cancers, malignant cells have demonstrated their manipulation and deregulation of translation to promote oncogenic activity[39]. One means of high jacking translational systems has been through mutations in ribosomal proteins. The concept of an 'oncogenic ribosome' has generated growing interest given the frequency of ribosomal protein mutations in cancer, the heterogeneity and plasticity reported in ribosomal composition and function, as well as its regulation of processes such as cell-cycle, migration, metabolism and cell growth[65]. It is this multifunctionality, and their potential role in cellular processes often hijacked in cancer, that make ribosomal proteins a novel topic of research in cancer development and progression[40]. Understanding how ribosomal protein mutations, which usually induce hypo-proliferative defects, can drive cellular transition to a disease characterized by uncontrolled cellular division is one of the outstanding questions in the field. Our mouse model, harboring the most common *RPS15* mutation in CLL patients, demonstrates that ribosomal mutations are capable of driving malignancy, impacting cell fate and function, and dysregulating cellular pathways.

Longitudinal observation of our conditional expression *Rps15*-S138F CD19-Cre mice demonstrated that *RPS15* mutations are capable of driving CLL-like disease (**Fig. 3**). Within the single mutant mouse population, we only observed disease progression within the *RPS15*^{Het} group

(10 out of 40 mice). This is consistent with mutations found in patients, where only heterozygous *RPS15* mutations have been described (**Table 1**). Additionally, *RPS15*^{Het}, double mutant and *Trp53*^{Het} mice with CLL-like disease presented unmutated IGHV segments, consistent with *Rps15*-MT patients (**Table 1 and Supplementary Table 1**). In one double mutant mouse with CLL, the CDR3 sequence, the antigen binding region of the BCR, has also been identified in other CLL mouse models. This CDR3 sequence, CMRYGNYWYFDVW, has been identified in CLL samples from Eμ-TCL1 (Yan et al., 2006), MDR (Klein et al., 2010) and IKZF3 (Lazarian et al. 2019) mice (**Supplementary Table 1**)[2,66,67]. We only observed 1 mouse out of 30 with significant levels of CD5+ B220+ cells in the peripheral blood of *RPS15*^{Hom} mice. It should be of note that for normal murine B cells we observed a 50% reduction in circulating B cells of *RPS15*^{Hom} mice, while *RPS15*^{Het} mice showed the same levels as *RPS15*^{WT} mice (**Fig. 2a**). It is possible that this contributes to the reduced incidence of CLL development in these mice. Analysis of young mice allowed us to investigate the means by which these mutations were altering B cells and leading to the development of proliferative disease.

In the mouse model, our analysis of progenitor B cell subpopulations demonstrated the ability of these mutations to influence major cell fate decisions within the mature B cell populations of the mice. In the spleen, we observed opposite phenotypes in the marginal zone B cells populations of *RPS15*^{Het} and *RPS15*^{Hom} with a loss of MZ B cells in the former and gain in the latter, as compared to *RPS15*^{WT} mice (**Fig. 2d**). We also observed a significant loss of B1a cells in the peritoneal cavity of *RPS15*^{Het} mice and an even more drastic decrease in *RPS15*^{Hom} mice (**Fig. 2f**). This directly contrasts the results observed in mice that developed CLL-like disease, where we see CD5+ B220+ cells making up the largest population of CLL cells within any organ, ranging from 26.2 to 92.5 percent of lymphocytes (**Fig. 3b**). It is possible that signals that monitor

ribosomal stress are driving increases levels of cell death and thus decreases in proliferation within the B1a population in these mice. This may position those cells that remain particularly poised for selective pressure to gain further mutations that overcome these mediators of cell death and lead to oncogenesis within the B1a population[68].

These deficiencies in proliferation and survival mediated by ribosomal protein mutations are further reinforced by the decreases in immune function observed. Both *RPS15*^{Het} and *RPS15*^{Hom} mice demonstrated low germinal center B cell formation after immunization with T-dependent antigen SRBC (**Fig. 2f**). Within the germinal center B cells undergo many rounds of proliferation in the event of an immune response[62]. It is possible that the same systems monitoring cell cycle regulation and proliferation within the B1a population are those preventing the levels of GC B cells from developing during an immune response. These observations may also show that those with *RPS15* mutations are more immunocompromised due to deficiencies in their adaptive immune response.

Given that a major determinant of marginal zone versus follicular B cell fate is the strength of BCR signaling we looked into how changes to receptor signaling may be driving the observed phenotypes[63]. The results of IgM stimulation on BCR signaling showed little changes in early signaling proteins across all three genotypes. Interestingly, we observed prolonged ERK activation following IgM stimulation in both mutant RPS15 genotypes (**Fig. 2g**). More investigation is necessary to understand why this is the case, however ERK signaling is directly upstream of Myc signaling, a pathway that repeatedly observed to be dysregulated in mutant *RPS15* cells (**Fig. 4**). Other groups have also observed that aberrant ERK activation is a means for ibrutinib resistance in diffuse large B-cell lymphoma (DBCL), another B cell malignancy[69]. Similarly, *RPS15*

mutations have been associated with ibrutinib resistance, while more work is necessary, this is a possible mechanism of action[36].

Even amongst growing evidence within patient cohorts that *RPS15* mutations function as an early driver in CLL development, the mechanisms that connect B cell dysregulation and the progression of disease remain elusive. Our data, expanding on patient data on the characteristics of *RPS15* mutations within CLL patients continued to exemplify the patterns previously described in the literature. Results from combined patient cohorts demonstrated the conserved localization of these mutations within the 14 amino acid regions of exon 4 in the C terminus of the protein (**Fig. 1a**). As noted, this region has been described as interacting within the A and P site of actively translating ribosomes[58,59]. Patient samples showed repetitive patterns of co-mutations such as 32% having *TP53* mutations, while 26% of patients without TP53 alterations had mutations in DNA-damage associated genes such as *ATM* and *POT1* (**Table 1**). These patterns further support the possible role for loss of DNA repair pathways in *RPS15*-mutated CLL.

Analysis of the cell pathways that are impacted by *RPS15* mutations elucidated shared patterns of dysregulation between patient samples, HG3 cell lines and murine B cells (**Fig. 4e**). Across all 3 cell types Myc targets were the most upregulated pathways in transcription. Furthermore, Ribosome profiling of *RPS15* mutant cells revealed broad changes in transcription and translation, particularly affecting Myc targets involved in rRNA and mRNA processing, translation, and protein modification.

In measuring TE of mRNA transcripts in HG3 cells, we detected a robust increase in TE of transcripts involved in p53 signaling and cell death. In *TP53* KO cells lines, however, such stress pathways were no longer induced, and we once again observed increased TE of Myc targets and ribosome-related transcripts. These findings suggest that *RPS15* mutation induces Myc-

mediated upregulation of ribosome synthesis, translation and protein modification – and that negative feedback mechanisms mediated by *TP53* may inhibit this response. Loss of *TP53* may thus serve to unmask this Myc-mediated phenotype. Indeed, such a signature would be in line with recent mechanistic studies that highlight the intricate cross-talk between Myc and p53, where Myc overexpression has been shown to induce p53-dependent apoptosis, and as a consequence, Myc-associated tumors often require disruption of the apoptosis pathway to promote cell proliferation[70].

There is accumulating evidence for ribosomal protein mediation in the regulation of Myc signaling. One study demonstrated that certain ribosomal proteins, including RPL11, can inhibit c-Myc mediated transcription by directly binding to c-Myc and inhibiting the recruitment of key co-activators (i.e. TRRAP) at c-Myc target gene promoters[70]. Additionally, *RPS14* has been described to inhibit c-Myc through similar mechanisms, and is also a regulator of cellular p53 stability by binding to MDM2. Haploinsufficiency of *RPS14* been identified in 5q-syndrome, an anemia due to the deletion on chromosome 5 that has an association with increases susceptibility to cancer[71]. In our own work, transcriptome analysis of CLL samples from *RPS15*^{Het} mice further support a role for cross talk between *RPS15* and c-Myc signaling. GSEA analysis of CLL samples compared to age-matched *RPS15*^{WT} controls revealed that the top upregulated pathways in CLL cells were Myc target genes. The next pathway identified was E2F Targets, further supporting the role of translational changes as seen in murine B cells and HG3 cells (**Fig. 4e and j**). It should be noted that Myc and E2F targets were identified as upregulated pathways in ribosomal profiling of *RPS15* mutant *TP53* KO HG3 cells, and RNA-seq from Primary CLL samples and Murine CLL samples (Figure 4).

These findings collectively indicate that the addition of *TP53* co-mutation, in conjunction with *RPS15* mutations cause changes through translational and Myc signaling pathways.

Additionally, this is supported by transcriptome analysis of 3-month *RPS15*^{Het} B cells, where we see the most down regulated pathway identified as Myc signaling targets (**Fig. 4c**). However, when *RPS15*^{Het} mice later develop CLL, this switches to the most upregulated pathway (**Fig. 4j**). This could mean that *RPS15* mutations alter c-Myc signaling, and the accumulation of co-mutations lead to up regulation of these targets and drive oncogenesis.

It is as yet unclear whether RPS15 mediates Myc activity through direct binding, or through downstream transcriptional activation of Myc and its associated pathways. In investigating the relationship between *RPS15* and MYC, we have identified that homozygous mutation of *RPS15* increases expression of the tyrosine kinase, ZAP70 (**Fig. 2h**). Recent work by others has shown that ZAP70 levels can directly influence Myc signaling, independent of BCR signaling[64]. We thus hypothesize that alterations to ZAP70 by *RPS15* mutations may then influence changes to Myc signaling, as we have seen consistently across *RPS15* mutated models. In future work, we will test this hypothesis, as well as determine whether RPS15 can directly bind c-Myc to affect transcription and whether mutation of *RPS15* influences such binding. Additionally, analysis of the proteome may detangle how translation impacts the transcripts identified by RNA-Seq and further uncover the connection between c-Myc and RPS15.

Chapter 3 Discussion and Perspectives

3.1 Conclusion

Together these findings from my thesis studies support a proposed model for the means by which ribosomal protein mutations in healthy cells are capable of driving cancer. This model suggests that in the presence of ribosomal protein mutations, high energy cell processes (i.e. protein synthesis) are tightly regulated and result in degradation of defective ribosomes[40]. Cells

carrying ribosomal protein mutations undergo negative selection unless a second hit occurs. RPS15 proteins are able to bind directly to MDM2 and stabilize p53, leading to cell cycle arrest and apoptosis. Altered levels of RPS15 protein lead to p53 stress responses, leading to deficiencies in DNA damage and repair processes create an environment largely susceptible to the acquisition of additional mutations[72].

In this case, new gene mutations suppress the surveillance system or enhances cell growth and proliferation. In line with this hypothesis, we report that the majority of patients with *RPS15* mutation also harbor a second mutation in genes involving DNA damage repair (i.e. *TP53*, *ATM* and *POT1*). Given the dysregulation of translation and evidence of Myc-mediated activation of pro-growth signals across our *RPS15* mutant models, as well as the ability of $RPS15^{Het}$ mutations to drive oncogenesis *in vivo,* these findings further support the concept of 'oncogenic ribosomes' and support the success of ribosomal targeted therapeutics in treatment of cancer[73].

3.2 Future Directions

The next steps in this research will be further characterization of the CLL-like disease identified in these mice. While we have confirmation by pathology, and demonstration of altered morphological features with RPS15-TP53 double mutant mice. WGS of murine CLL samples will show what additional mutations were accrued in the progression of normal B cells into malignant cells. Mutations recurring within individual genes across samples or within common pathways, like those noted above may provide further insight into how *RPS15* drives CLL. Additionally, we will be able to determine the fidelity in which our murine CLL recapitulates patients' disease. Finally, following our analysis of the transcriptome and proteome of murine B cells harboring *RPS15* mutations, the next step is to look at the translational landscape. Riboseq analysis allows

for understanding changing to reading transcripts within actively translating ribosomes. These findings can provide insight into translational efficiency of ribosomes harboring mutant *RPS15.* In cell lines we observed increased utilization of canonical ORFs as opposed to non-canonical ORFs, pseudogenes and lncRNAs. Of these canonical ORFs, we detected a robust increase in TE of transcripts involved in p53 signaling and cell death. In *TP53* KO cells lines, however, such stress pathways were no longer induced, and we once again observed increased TE of Myc targets and ribosome-related transcripts.

Moving forward with this work, it remains critical to develop a better mechanistic understanding between RPS15, TP53 and MYC. Further identifying the means of regulation that these proteins have on one another may help identify the most useful therapeutics for patients harboring *Rps15* mutations. Additionally, this may broaden the understanding of how RP mutations drive oncogenesis in a number of other malignancies. Following this study, a number of questions remain open. One major question is why *RPS15* mutations specifically impact B cells. While ribosomal mutations have been described in other cancers as well as ribosomopathies that lead to susceptibility to cancer, *RPS15* mutations have only been described as recurring in CLL[74]. It is not yet understood what makes B cells predisposed to acquiring these mutations or why these mutations have the ability to drive cancer development within B cells. As we gain a better understanding of the mechanisms behind mutant *RPS15,* further investigations may begin to address how such mechanisms lead to therapeutic resistance and decreases in progression free survival.

3.3 Limitations

The major limitations within this research fall within the physiologic differences between mice and humans. While this model allows for greater complexity and biologic relevance than cell lines, there remains major differences between humans and mice. CLL is a disease that primarily effects the elderly population, while we observed CLL development in aged mice, the impact of aging over the course of 2 years is likely much different than the 70 years experienced by humans. The acquisition of this mutation also differs from what is seen in patients. These mice acquire mutated *RPS15* during B cell development, when the mice are born all mature B cells harbor the mutant gene. In humans, it is likely that this mutation is acquired over the course of a person's lifetime, additionally it is acquired in a single B cell that then becomes malignant. While we cannot perfectly model the ways the disease develops in humans, this model provides the most similar means to date that we can study the impact of these mutations on an organism.

3.4 Perspectives in the field

Within the field of oncology, further accessibility and improvement of genomic sequencing gives physicians an up-close look at a patients' cancer cells. The ability to look at a total clonal population and identify those mutations driving proliferation and therapeutic resistance can become a tool for physicians to tailor treatments from patient to patient. I believe that in CLL in particular, an indolent disease with low mutational burden, treatments will continue to move further toward personalized treatment regimens. Global collaborations on the identification of driver mutations amongst the greater CLL population allow for a greater understanding of the outcomes and patterns of progression a patient may experience. These advancements, alongside functional studies that detangle the mechanistic alterations driven by these mutations within the

cell, help create a deeper understanding into the specific malignancies ailing a patient. Together, we can envision that a deeper understanding of an individual's cancerous cells can act as an instruction guide toward the best course of treatment against the disease. The answer towards personalized medicine remains within an open communication and collaboration between clinicians and researchers. Understanding the incidence of relapse and therapeutic resistance generates open questions and a guide for investigation for researchers to further dive into the why and by what means can they be addressed.

Innovations within the field of research have also aided scientists in more closely modeling the findings from patients in a lab setting. Continuous improvement in the field of genetic manipulation gives researchers the ability to model genetic alterations that have been identified in humans, in cells lines and *in vivo* modeling. In our studies we were able to observe how genetic alterations in a single cell type, B cells, impacted the entire organism. This could be observed in the compensation of larger T cell populations in the *RPS15*^{Hom} mice that was seen alongside the 50% reduction in B cells. Improved modeling that is able to more closely resemble the alterations observed in humans can greatly impact the fidelity and accuracy that results generated in the lab will translate to the human population.

By improving upon these models, we can further investigate therapeutic options to treat CLL, as well as other ribsosomopathies. There are a number of small molecule targets that act upon the structural integrity of rRNA to manipulate ribosomal integrity[75]. Additionally targeting components of ribosomal maturation may allow for the specific targeting of aberrant ribosomes[76]. In the context of CLL, a clonally heterogenous disease, therapeutic plans driving evolutionary herding have been described[3]. Improved understanding of the phenotypes that arise with the presence of specific mutations allow for these to become targetable. These methods require a

robust understanding of the clonal dynamics behind CLL and how to drive stable clones. Using these models to understand the phenotype and mechanisms underlying *RPS15* mutations help to improve the greater understanding of CLL and how we can advance personalized treatment regimens for patients.

Supplementary Figure 3: **Impact of *TP53* co-mutations**

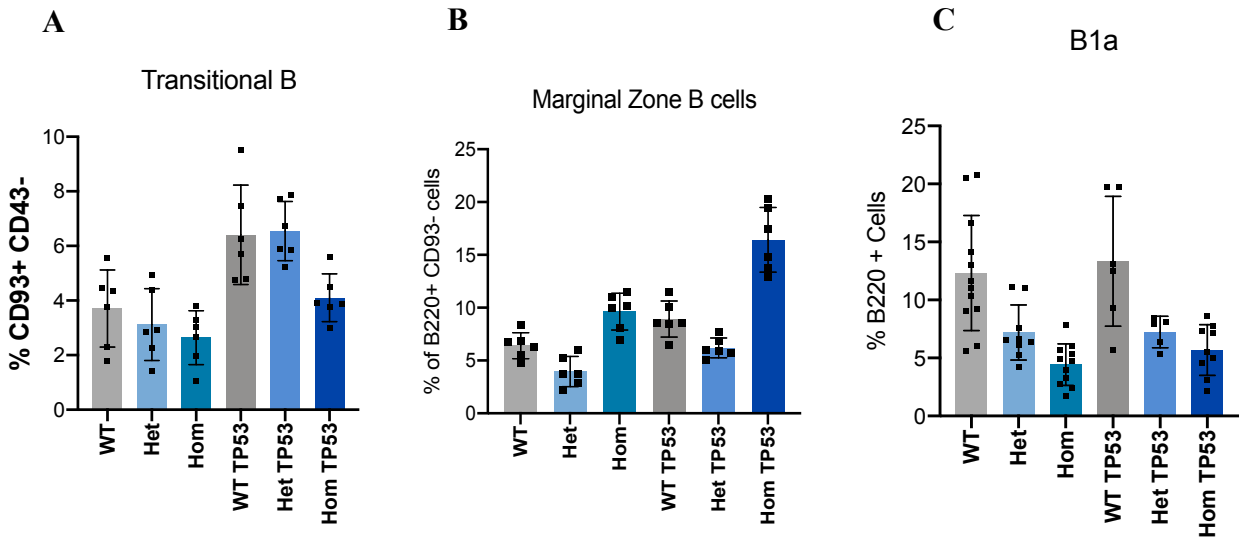

(a)Percentages of transitional B cells present in bone marrow of *Rps15*^{WT}, *RPS15*^{het} and *RPS15*^{hom} (+/- TP53^{Het}) mice (n=6). Data represent Mean±SEM and were compared using one-way ANOVA followed by Tukey's multiple comparison test.
(b) Percentages of marginal zone B cells present in spleen of *Rps15*^{WT}, *RPS15*^{het} and *RPS15*^{hom} (+/- TP53^{Het}) mice (n=6). Data represent Mean±SEM and were compared using one-way ANOVA followed by Tukey's multiple comparison test.
(c) Percentages of B1a cells present in peritoneum of *Rps15*^{WT}, *RPS15*^{het} and *RPS15*^{hom} (+/- TP53^{Het}) mice (B1a, n=12, TP53 mice, n=6). Data represent Mean±SEM and were compared using one-way ANOVA followed by Tukey's multiple comparison test.

Supplementary Figure 4: **B cell Development**

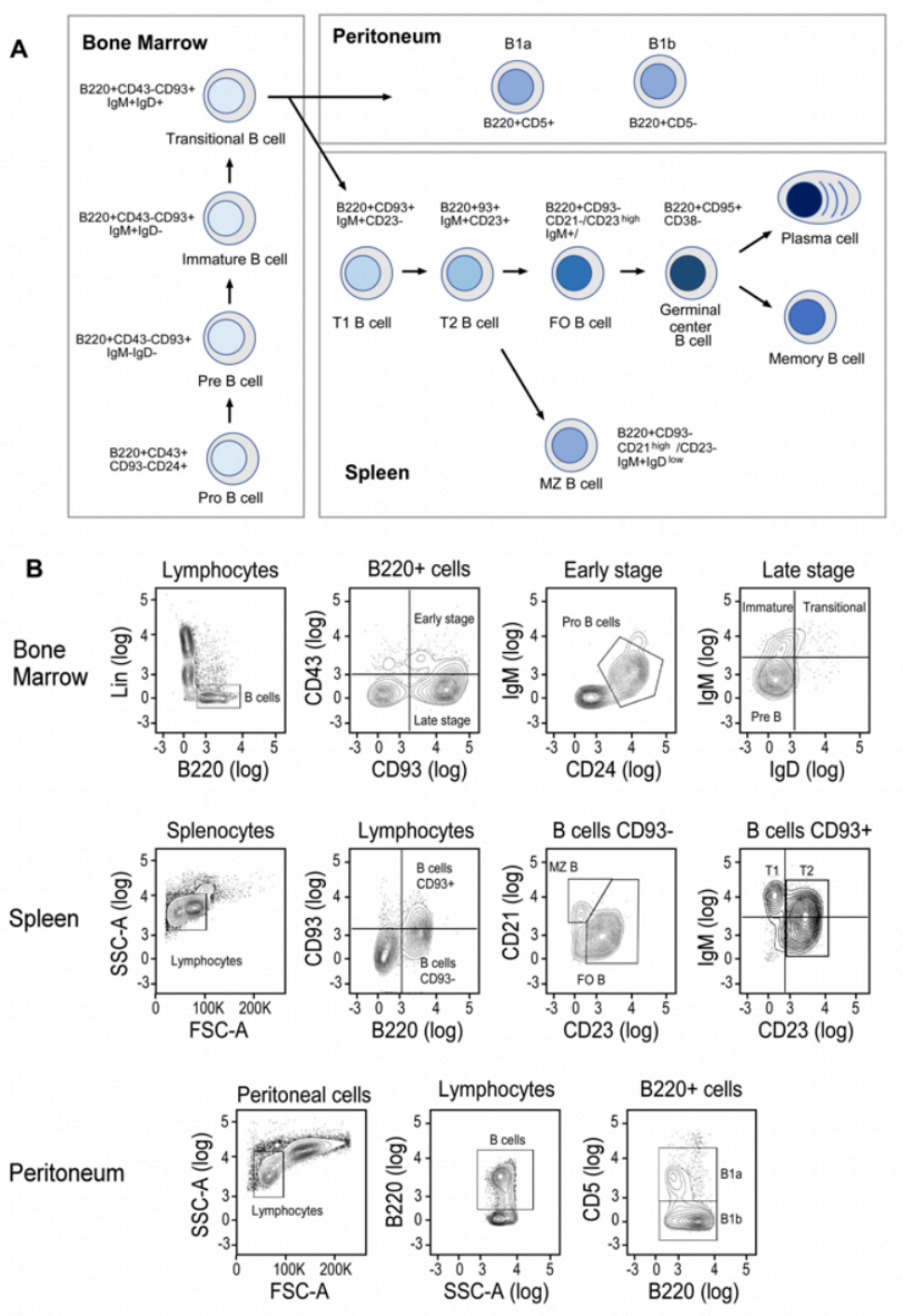

Supplemental Figure 4[2] - Published in Lazarian et. al. 2021

(a) Schema of B cell development, including cell surface markers of B cell sub populations, in bone marrow, spleen and peritoneal cavity.

(b) Gating strategy for flow cytometry and quantification for subsets of B cells during development in in bone marrow, spleen and peritoneal cavity

Supplementary Table 1. Sequence analysis of the dominant productive IGHV rearrangement of CLL mice obtained by NGS sequencing.

Supplementary Table 1| Sequence analysis of the dominant productive Igh rearrangement of CLL/DLBCL mice obtained by NGS sequencing.

Alias	Genotype	Source	CDR3	CDR3 length	V-gene	D-gene	J-gene	n reading	Rearrangement	%Identity	IGHV status	rearrangement sequence
RPS_1	RPS15 Het	PBMC	CARETGSYWYFDVW	12	IGHV1-55*01	IGHD4-1*01	IGHJ1*01	1	Productive IGH rearranged sequence (no stop codon and in-frame junction)	100%	UM	CCACACTGACTGTAGACACATCCTCCAGCACAGCCTACATGCAGCTCAGCAGCCTGACATCTGAGGACTCTGCGGTCTATTA
RPS_2	RPS15 Het	PBMC			IGHV6-6*01	IGHD2-13*01	IGHJ1*01	1	IGH rearranged sequence (but no junction found)	100%	UM	CTGAGTCTGTGAAAGGGAGGTTCACCATCTCAAGAGATGATTCCAAAAGTAGTGTCTACCTGCAAATGAACAGCTTAAGAGC
RPS_3	RPS15 Het	PBMC	CARGVYPYWYFDVW	12	IGHV1-52*01 or IGHV1-61*01 or IGHV1-69*01 or IGHV1-74*01	IGHD5-2*01	IGHJ1*01	1	Productive IGH rearranged sequence (no stop codon and in-frame junction)	100%	UM	CCACATTGACTGTAGACAAATCCTCCAGCACAGCCTACATGCAGCTCAGCAGCCTGACATCTGAGGACTCTGCGGTCTATTA
RPS_4	RPS15 Het	PBMC	CARDASNWDYAMDYW	13	IGHV7-1*01	IGHD2-5*01	IGHJ4*01	3	Productive IGH rearranged sequence (no stop codon and in-frame junction)	100%	UM	TCGTCTCCAGAGACACTTCCCAAAGCATCCTCTACCTTCAGATGAATGCCCTGAGAGCTGAGGACACTGCCATTTATTACTG
RPS_5	RPS15 Het	PBMC	CAYDYDWYFDVW	10	IGHV4-1*01 or IGHV4-2*01	IGHD2-4*01 or IGHD2-9*02	IGHJ1*01	3	Productive IGH rearranged sequence (no stop codon and in-frame junction)	100%	UM	ATAAATTCATCATCTCCAGAGACAACGCCAAAAATACGCTGTACCTGCAAATGAGCAAAGTGAGATCTGAGGACACAGCCCTT
RPS_6	RPS15 Het	PBMC	CARGGDFDYW	8	IGHV1-52*01 or IGHV1-61*01 or IGHV1S126*01	IGHD4-1*01 or	IGHJ2*03	2	Productive IGH rearranged sequence (no stop codon and in-frame junction)	100%	UM	TCAAGGACAAGGCCACATTGACTGTAGACAAATCCTCCAGCACAGCCTACATGCAGCTCAGCAGCCTGACATCTGAGGACTC
RPS_7	RPS15 Het	PBMC	CARETDGFYYFDYW	12	IGHV1-55*01	IGHD6-1*02	IGHJ2*01 or *02 or *03	3	Productive IGH rearranged sequence (no stop codon and in-frame junction)	100%	UM	CCACACTGACTGTAGACACATCCTCCAGCACAGCCTACATGCAGCTCAGCAGCCTGACATCTGAGGACTCTGCGGTCTATTA
RPS_8	RPS15 Het	PBMC	CARSYGYAMDYW	10	IGHV8-12*01	IGHD1-1*01	IGHJ4*01	3	Productive IGH rearranged sequence (no stop codon and in-frame junction)	100%	UM	GCCGGCTCACAATCTCCAAGGATACCTCCAGAAACCAGGTATTCCTCAAGATCACCAGTGTGGACACTGCAGATACTGCCAC
DM1	RPS15 Het TP53	PBMC	CMRYSNYWYFDVW	11	IGHV11-2*01	IGHD2-5*01	IGHJ1*01	3	Productive IGH rearranged sequence (no stop codon and in-frame junction)	100%	UM	GATTCACTATCTTCAGAGACAATGACAAGAGCACCCTGTACCTGCAGATGAGCAATGTGCGATCGGAGGACACAGCCACGTA
DM2	RPS15 Het TP53	PBMC	CARDITTVVDWYFDVW	14	IGHV5-4*01 or *03	IGHD1-1*01	IGHJ1*01	1	Productive IGH rearranged sequence (no stop codon and in-frame junction)	100%	UM	TCTCCAGAGACAATGCCAAGAACAACCTGTACCTGCAAATGAGCCATCTGAAGTCTGAGGACACAGCCATGTATTACTGTGC
DM3	RPS15 Het TP53	PBMC	CMRYGNYWYFDVW	11	IGHV11-2*01	IGHD1-1*02	IGHJ1*01	3	Productive IGH rearranged sequence (no stop codon and in-frame junction)	100%	UM	GATTCACTATCTTCAGAGACAATGACAAGAGCACCCTGTACCTGCAGATGAGCAATGTGCGATCGGAGGACACAGCCACGTA
TP1	TP53 Het	PBMC			IGHV6-3*01	IGHD1-1*01	IGHJ1*01	N/A	IGH rearranged sequence (but no junction found)	100%	UM	AAGGGAGGTTCACCATCTCAAGAGATGATTCCAAAAGTAGTGTCTACCTGCAAATGAACAACTTAAGGGCTGAAGACACTGG
TP2	TP53 Het	PBMC	CARLWYAMDYW	9	IGHV1-9*01	IGHD1-1*02	IGHJ4*01	2	Productive IGH rearranged sequence (no stop codon and in-frame junction)	100%	UM	AGGGCAAGGCCACATTCACTGCAGATACATCCTCCAACACAGCCTACATGCAACTCAGCAGCCTGACAACTGAGGACTCTGC

Sequence were subjected to analysis using IMGT/Vquest software to define all V, D and J genes as well as CDR3 sequence

PBMC: peripheral blood mononuclear cells; PC : peritoneum cavity; M: mutated; UM: unmutated

* CDR3 sequence also found in Eμ-TCL1 (Yan et al., 2006) and MDR (Klein et al., 2010) mice

Chapter 4 Bibliography

Bibliography

1. Landau, D. A. *et al.* Mutations driving CLL and their evolution in progression and relapse. *Nature* (2015). doi:10.1038/nature15395
2. Lazarian, G. *et al.* A hotspot mutation in transcription factor IKZF3 drives B cell neoplasia via transcriptional dysregulation. *Cancer Cell* **39**, 380-393.e8 (2021).
3. Gutierrez, C. & Wu, C. J. Clonal dynamics in chronic lymphocytic leukemia. *Blood Advances* (2019). doi:10.1182/bloodadvances.2019000367
4. Puente, X. S. *et al.* Non-coding recurrent mutations in chronic lymphocytic leukaemia. *Nature* (2015). doi:10.1038/nature14666
5. Ljungström, V. *et al.* Whole-exome sequencing in relapsing chronic lymphocytic leukemia: Clinical impact of recurrent RPS15 mutations. *Blood* (2016). doi:10.1182/blood-2015-10-674572
6. Knisbacher, B. A. *et al.* The CLL-1100 Project: Towards Complete Genomic Characterization and Improved Prognostics for CLL. *Blood* **136**, 3–4 (2020).
7. Hossfeld, D. K. World Health Organization Classification of Tumours: Pathology and Genetics of Tumours of Haematopoietic and Lymphoid Tissues. *Ann. Oncol.* (2002). doi:10.1093/annonc/mdf146
8. Swerdlow, S. H. *et al.* The 2016 revision of the World Health Organization classification of lymphoid neoplasms. *Blood* (2016). doi:10.1182/blood-2016-01-643569
9. Surveillance, Epidemiology, and E. R. (SEER) P. Chronic Lymphocytic Leukemia - Cancer Stat Facts. *SEER* (2020).
10. Abrisqueta, P. *et al.* Improving survival in patients with chronic lymphocytic leukemia

(1980-2008): the Hospital Clínic of Barcelona experience. *Blood* **114**, 2044–2050 (2009).

11. Lingamaneni, P. *et al.* Outcomes of Patients with Chronic Lymphocytic Leukemia Admitted with Sepsis: An Analysis of National Inpatient Sample Database. *Blood* **134**, 5460–5460 (2019).
12. Skarbnik, A. P. & Faderl, S. The role of combined fludarabine, cyclophosphamide and rituximab chemoimmunotherapy in chronic lymphocytic leukemia: current evidence and controversies. *Ther. Adv. Hematol.* (2017). doi:10.1177/2040620716681749
13. Rai, K. R. 1 Progress in chronic lymphocytic leukaemia: A historical perspective. *Baillieres. Clin. Haematol.* (1993). doi:10.1016/S0950-3536(05)80174-X
14. Sagatys, E. M. & Zhang, L. Clinical and laboratory prognostic indicators in chronic lymphocytic leukemia. *Cancer Control* (2012). doi:10.1177/107327481201900103
15. Definition of progression-free survival - NCI Dictionary of Cancer Terms - National Cancer Institute. Available at: https://www.cancer.gov/publications/dictionaries/cancer-terms/def/progression-free-survival. (Accessed: 29th March 2021)
16. Dürig, J. *et al.* ZAP-70 expression is a prognostic factor in chronic lymphocytic leukemia. *Leukemia* (2003). doi:10.1038/sj.leu.2403147
17. Ding, W. *et al.* Correlation Between Peripheral Blood Counts and Extent of Bone Marrow Infiltration in Chronic Lymphocytic Leukemia. *Blood* **126**, 2926–2926 (2015).
18. Moreno, C. *et al.* Ibrutinib plus obinutuzumab versus chlorambucil plus obinutuzumab in first-line treatment of chronic lymphocytic leukaemia (iLLUMINATE): a multicentre, randomised, open-label, phase 3 trial. *Lancet Oncol.* **20**, 43–56 (2019).
19. Burger, J. A. & Chiorazzi, N. B cell receptor signaling in chronic lymphocytic leukemia. (2013). doi:10.1016/j.it.2013.07.002

20. Byrd, J. C. *et al.* Acalabrutinib (ACP-196) in Relapsed Chronic Lymphocytic Leukemia. *N. Engl. J. Med.* **374**, 323–332 (2016).

21. Anurathapan, U. *et al.* Kinetics of tumor destruction by chimeric antigen receptor-modified T cells. *Mol. Ther.* (2014). doi:10.1038/mt.2013.262

22. Burger, J. Treatment of Chronic Lymphocytic Leukemiao Title. *N. Engl. J. Med.* **383**, (202AD).

23. Korz, C. *et al.* Evidence for distinct pathomechanisms in B-cell chronic lymphocytic leukemia and mantle cell lymphoma by quantitative expression analysis of cell cycle and apoptosis-associated genes. *Blood* **99**, 4554–4561 (2002).

24. Fraietta, J. A. *et al.* Determinants of response and resistance to CD19 chimeric antigen receptor (CAR) T cell therapy of chronic lymphocytic leukemia. *Nat. Med.* **24**, 563–571 (2018).

25. Gauthier, J. *et al.* Feasibility and efficacy of CD19-targeted CAR T cells with concurrent ibrutinib for CLL after ibrutinib failure. in *Blood* **135**, 1650–1660 (American Society of Hematology, 2020).

26. Krämer, I. *et al.* Allogeneic hematopoietic cell transplantation for high-risk CLL: 10-year follow-up of the GCLLSG CLL3X trial. *Blood* **130**, 1477–1480 (2017).

27. Parikh, S. A., Kay, N. E. & Shanafelt, T. D. How we treat Richter syndrome. *Blood* (2014). doi:10.1182/blood-2013-11-516229

28. Yin, S. *et al.* A Murine Model of Chronic Lymphocytic Leukemia Based on B Cell-Restricted Expression of Sf3b1 Mutation and Atm Deletion. *Cancer Cell* (2019). doi:10.1016/j.ccell.2018.12.013

29. Bichi, R. *et al.* Human chronic lymphocytic leukemia modeled in mouse by targeted

TCL1 expression. *Proc. Natl. Acad. Sci. U. S. A.* (2002). doi:10.1073/pnas.102181599

30. Hamblin, T. J. The TCL1 mouse as a model for chronic lymphocytic leukemia. *Leukemia Research* (2010). doi:10.1016/j.leukres.2009.08.004

31. High throughput single-cell detection of multiplex CRISPR-edited gene modifications. | Mission Bio. Available at: https://missionbio.com/resources/publications/ten-hacken-genome-biology-2020/. (Accessed: 31st March 2021)

32. Landau, D. A. *et al.* Mutations driving CLL and their evolution in progression and relapse. *Nature* (2015). doi:10.1038/nature15395

33. Yu, L. *et al.* Survival of Del17p CLL depends on genomic complexity and somatic mutation. *Clin. Cancer Res.* (2017). doi:10.1158/1078-0432.CCR-16-0594

34. Braschi, B. *et al.* Genenames.org: The HGNC and VGNC resources in 2019. *Nucleic Acids Res.* (2019). doi:10.1093/nar/gky930

35. Ljungström, V. & Rosenquist, R. Not so lost in translation: RPS15 mutations in CLL. *Blood* (2018). doi:10.1182/blood-2018-09-875179

36. Bretones, G. *et al.* Altered patterns of global protein synthesis and translational fidelity in RPS15-mutated chronic lymphocytic leukemia. *Blood* (2018). doi:10.1182/blood-2017-09-804401

37. Burger, J. A. *et al.* Clonal evolution in patients with chronic lymphocytic leukaemia developing resistance to BTK inhibition. *Nat. Commun.* (2016). doi:10.1038/ncomms11589

38. Ljungström, V. *et al.* Whole-exome sequencing in relapsing chronic lymphocytic leukemia: Clinical impact of recurrent RPS15 mutations. *Blood* **127**, 1007–1016 (2016).

39. Robichaud, N., Sonenberg, N., Ruggero, D. & Schneider, R. J. Translational control in

cancer. *Cold Spring Harb. Perspect. Biol.* (2019). doi:10.1101/cshperspect.a032896

40. Goudarzi, K. M. & Lindström, M. S. Role of ribosomal protein mutations in tumor development (Review). *International Journal of Oncology* (2016). doi:10.3892/ijo.2016.3387

41. Boisvert, F. M., Van Koningsbruggen, S., Navascués, J. & Lamond, A. I. The multifunctional nucleolus. *Nature Reviews Molecular Cell Biology* (2007). doi:10.1038/nrm2184

42. Panić, L., Montagne, J., Cokarić, M. & Volarević, S. S6-haploinsufficiency activates the p53 tumor suppressor. *Cell Cycle* (2007). doi:10.4161/cc.6.1.3666

43. McGowan, K. A. *et al.* Ribosomal mutations cause p53-mediated dark skin and pleiotropic effects. *Nat. Genet.* (2008). doi:10.1038/ng.188

44. Anderson, S. J. *et al.* Ablation of Ribosomal Protein L22 Selectively Impairs αβ T Cell Development by Activation of a p53-Dependent Checkpoint. *Immunity* (2007). doi:10.1016/j.immuni.2007.04.012

45. S.O., S. *et al.* Bypass of the pre-60S ribosomal quality control as a pathway to oncogenesis. *Proc. Natl. Acad. Sci. U. S. A.* (2014).

46. Sanjana, N. E., Shalem, O. & Zhang, F. Improved vectors and genome-wide libraries for CRISPR screening. *Nature Methods* (2014). doi:10.1038/nmeth.3047

47. Doench, J. G. *et al.* Rational design of highly active sgRNAs for CRISPR-Cas9-mediated gene inactivation. *Nat. Biotechnol.* (2014). doi:10.1038/nbt.3026

48. Quijada Álamo, M. *et al.* CRISPR/Cas9-Generated Models Uncover Therapeutic Vulnerabilities of Del(11q) Chronic Lymphocytic Leukemia Cells to Dual BCR and PARP Inhibition. *Blood* (2018). doi:10.1182/blood-2018-99-116080

49. Heckl, D. *et al.* Generation of mouse models of myeloid malignancy with combinatorial genetic lesions using CRISPR-Cas9 genome editing. *Nat. Biotechnol.* (2014). doi:10.1038/nbt.2951

50. García-Tuñón, I. *et al.* The CRISPR/Cas9 system efficiently reverts the tumorigenic ability of BCR/ABL in vitro and in a xenograft model of chronic myeloid leukemia. *Oncotarget* (2017). doi:10.18632/oncotarget.15215

51. Brinkman, E. K., Chen, T., Amendola, M. & Van Steensel, B. Easy quantitative assessment of genome editing by sequence trace decomposition. *Nucleic Acids Res.* (2014). doi:10.1093/nar/gku936

52. Dobin, A. *et al.* STAR: Ultrafast universal RNA-seq aligner. *Bioinformatics* (2013). doi:10.1093/bioinformatics/bts635

53. Love, M. I., Huber, W. & Anders, S. Moderated estimation of fold change and dispersion for RNA-seq data with DESeq2. *Genome Biol.* (2014). doi:10.1186/s13059-014-0550-8

54. Subramanian, A. *et al.* Gene set enrichment analysis: A knowledge-based approach for interpreting genome-wide expression profiles. *Proc. Natl. Acad. Sci. U. S. A.* (2005). doi:10.1073/pnas.0506580102

55. Li, B. & Dewey, C. N. RSEM: Accurate transcript quantification from RNA-Seq data with or without a reference genome. *BMC Bioinformatics* (2011). doi:10.1186/1471-2105-12-323

56. McGlincy, N. J. & Ingolia, N. T. Transcriptome-wide measurement of translation by ribosome profiling. *Methods* (2017). doi:10.1016/j.ymeth.2017.05.028

57. Chothani, S. *et al.* deltaTE: Detection of Translationally Regulated Genes by Integrative Analysis of Ribo-seq and RNA-seq Data. *Curr. Protoc. Mol. Biol.* (2019).

doi:10.1002/cpmb.108

58. Graifer, D. & Karpova, G. Structural and functional topography of the human ribosome. *Acta Biochimica et Biophysica Sinica* (2012). doi:10.1093/abbs/gmr118

59. Khairulina, J. *et al.* Eukaryote-specific motif of ribosomal protein S15 neighbors A site codon during elongation and termination of translation. *Biochimie* (2010). doi:10.1016/j.biochi.2010.02.031

60. Lebien, T. W., Thomas, * & Tedder, F. B lymphocytes: how they develop and function. (2008). doi:10.1182/blood

61. Wang, K., Wei, G. & Liu, D. *CD19: a biomarker for B cell development, lymphoma diagnosis and therapy*. (2012). doi:10.1186/2162-3619-1-36

62. Abbas K. Abul, Litchman H. Andrew, P. S. *Cellular and Molecular Immunology NINTH EDITION*. *Hilos Tensados* (2019).

63. Cariappa, A. *et al.* The Follicular versus Marginal Zone B Lymphocyte Cell Fate Decision Is Regulated by Aiolos, Btk, and CD21. *Immunity* **14**, 603–615 (2001).

64. Chen, J. *et al.* ZAP-70 constitutively regulates gene expression and protein synthesis in chronic lymphocytic leukemia. *Blood* (2021). doi:10.1182/blood.2020009960

65. Bastide, A. & David, A. The ribosome, (slow) beating heart of cancer (stem) cell. *Oncogenesis* **7**, 34 (2018).

66. Klein, U. *et al.* The DLEU2/miR-15a/16-1 Cluster Controls B Cell Proliferation and Its Deletion Leads to Chronic Lymphocytic Leukemia. *Cancer Cell* **17**, 28–40 (2010).

67. Yan, X.-J. *et al. B cell receptors in TCL1 transgenic mice resemble those of aggressive, treatment-resistant human chronic lymphocytic leukemia*. (2006).

68. Sulima, S. O., Hofman, I. J. F., De Keersmaecker, K. & Dinman, J. D. How Ribosomes

Translate Cancer. *Cancer Discov.* **7**, 1069 LP – 1087 (2017).

69. Chen, J. G. *et al.* BTK Cys481Ser drives ibrutinib resistance via ERK1/2 and protects BTK wild-type MYD88-mutated cells by a paracrine mechanism. *Blood* (2018). doi:10.1182/blood-2017-10-811752

70. Dai, M. S. & Lu, H. Crosstalk between c-Myc and ribosome in ribosomal biogenesis and cancer. *Journal of Cellular Biochemistry* (2008). doi:10.1002/jcb.21895

71. Zhou, X., Hao, Q., Liao, J., Liao, P. & Lu, H. Ribosomal Protein S14 Negatively Regulates c-Myc Activity*. *J. Biol. Chem.* **288**, 21793–21801 (2013).

72. Daftuar, L., Zhu, Y., Jacq, X. & Prives, C. Ribosomal Proteins RPL37, RPS15 and RPS20 Regulate the Mdm2-p53-MdmX Network. *PLoS One* **8**, (2013).

73. Gilles, A. *et al.* Targeting the Human 80S Ribosome in Cancer: From Structure to Function and Drug Design for Innovative Adjuvant Therapeutic Strategies. *Cells* (2020). doi:10.3390/cells9030629

74. Kampen, K. R., Sulima, S. O., Vereecke, S. & De Keersmaecker, K. Hallmarks of ribosomopathies. *Nucleic acids research* (2020). doi:10.1093/nar/gkz637

75. Bidou, L., Allamand, V., Rousset, J. P. & Namy, O. Sense from nonsense: Therapies for premature stop codon diseases. *Trends in Molecular Medicine* (2012). doi:10.1016/j.molmed.2012.09.008

76. Silvera, D., Formenti, S. C. & Schneider, R. J. Translational control in cancer. *Nature Reviews Cancer* (2010). doi:10.1038/nrc2824